AIMS Mathematics, 10(9): 20312–20345.
DOI:10.3934/math.2025908
Received: 01 July 2025
Revised: 27 August 2025
Accepted: 29 August 2025
Published: 05 September 2025

https://www.aimspress.com/journal/Math

Research article

Numerical investigation of a wireless sensor network epidemic model with α-stable noise: A case study

Hassan Tahir[1,2], **Anwarud Din**[3], **Wajahat Ali Khan**[4] **and Mati ur Rahman**[5,*]

[1] MSU-BIT-SMBU Joint Research Center of Applied Mathematics, Shenzhen MSU-BIT University, Shenzhen, China
[2] School of Mathematics and Statistics, Beijing Institute of Technology, Beijing, China
[3] Department of Mathematics, Sun Yat-sen University, Guangzhou 510275, China
[4] Department of Mathematics, University of Malakand, Chakdara 18800, KPK, Pakistan
[5] Department of Mathematics and Statistics, College of Science, Imam Mohammad Ibn Saud Islamic University (IMSIU), Riyadh, Saudi Arabia

* **Correspondence:** Email: mrmahman@imamu.edu.sa.

Abstract: This study examines a stochastic susceptible-exposed-infected-recovered-vaccinated ($\mathbf{SE_1E_2IRV}$) model exhibiting the dynamics of the computer virus within the wireless sensor networks (WSNs) while considering the unpredictability of nodes and the impact of anti-virus measures. The model is formulated with reasonable assumptions, and the stochastic stability is performed with a derivation of a six-dimensional Fokker-Planck equation. To obtain an analytical representation of the probability density functions, a scheme is developed and subsequently implemented in MATLAB. The behavior of the model around the quasi-endemic state is numerically investigated, which reflects the main objective and unique novelty of the present work. On the basis of various parameter settings, graphical illustrations of the model are presented showing the authenticity of the analytical results and complex aspects of the phenomenon. The paper concludes with a brief summary of the study and important insights for future research.

Keywords: computer virus model; wireless sensor networks; Lévy noise; Fokker-Planck equation; numerical simulation
Mathematics Subject Classification: 60G51, 60H10, 92D30

1. Introduction

The advancement of information technology (IT) directly relates to the potential risks associated with wireless sensor networks. Such advancements are causing significant harm to human lives

as well as posing enormous threats to global security. The IT users of this modern era demand a network with key desirable properties like efficiency, security, and reliability. In a wireless network, a sensor node is a compact, innovative, and low-cost device. WSNs have applications in a variety of fields, including mission-critical installations and continuous data collection. These networks are essential in various applications, including agricultural object inspection, military targeting, flood identification, disaster prevention, environmental systems, pollution-related surveillance, exploration of hazardous environments, traffic monitoring, gas monitoring, vehicle tracking, seismic sensing, healthcare applications, and water quality monitoring (Akyildiz, Su Sankarasubramaniam, [1–3]). Despite that sensor nodes are very economical and clever devices, nonetheless, they are limited by resources such as limited battery life, memory, and computing power [4, 5]. As a result, the combination of restricted resources and decentralized design in wireless sensor networks creates substantial challenges for establishing wireless connections and guaranteeing acceptable network security. Wireless sensor networks are inherently more vulnerable to threats than other networks, making them easier for virus attacks [6]. Despite deploying various security measures to secure the network, hackers may still exploit software vulnerabilities and faults, posing persistent risks.

The growing prevalence of persistent multi-malware attacks on WSNs has motivated computer scientists and mathematicians to understand and investigate the complex dynamics of network nodes by employing the tools of mathematical modeling. Such modeling and studying the underlying dynamics of the problem can help us to illustrate the simultaneous influence of malicious signals and virus strains on the nodes as well as to predict, analyze, and mitigate such threats. Further, models are very helpful in understanding the vulnerabilities and risks associated with the dynamics of these viruses and can effectively explain their intrinsic properties. The performance of a WSN can be affected by numerous factors. Malware attacks can cause sensor nodes to perform unnecessary excessive computation or communication tasks, thereby consuming more energy. Different kinds of malware generate energy-intensive operations that quickly deplete a node's battery, potentially causing node failure or even network disturbance [7, 8]. These attacks also target critical components of sensor nodes, including memory, CPU, and communication bandwidth. Nowadays, a huge number of malware are present within WSNs to compete for these resources, potentially leading to resource depletion and disruption of regular network operations. Software vulnerabilities can arise from a variety of factors, including faulty coding, defects in system architecture, and insufficient security mechanisms. These challenges are unavoidable in the context of WSNs. Due to the restricted communication range of WSN sensor nodes, multi-hop data transfer is required [7]. These limitations restrict the ability of nodes to fight against viral assaults, including those that are triggered by the worms, the worms themselves, and related malicious software [8]. The long-term survival of the network relies on its capacity to efficiently control and manage worm reproduction. Understanding and managing these risks in WSNs is strongly dependent on researching the propagation of malicious signals, and mathematical modeling emerges as the most effective method for assessing and limiting their spread [9–12]. Recent advances in secure control strategies, anomaly detection, and intrusion detection for networked and sensor-based systems have been reported in the literature [13–16]. A typical wireless sensor network is illustrated in Figure 1.

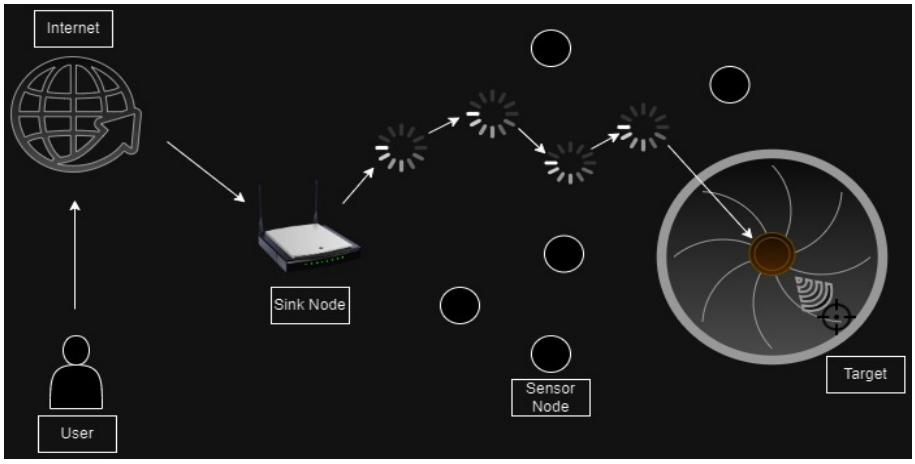

Figure 1. Schematic representation of WSN.

The methods of mathematical modeling for predicting the dynamic behavior of infectious diseases are rigorous and straightforward, facilitating researchers to forecast the future trends and root causes of the epidemic diseases [17–19]. Extreme moistness, precipitation, and ambient temperature significantly influence the dynamic patterns of nearly all human epidemics. Given this significant component of randomness, a deterministic model may be readily converted to a stochastic model that incorporates these environmental uncertainties. These disturbances include variations in parameters due to the environment and random noise arising from the differential systems [20–22]. Furthermore, several researchers have demonstrated that stochastic modeling is more beneficial than deterministic modeling, as it provides an additional degree of freedom. Population dynamics and epidemic models subject to randomness via white noise have a rich literature; the readers are suggested to see [23, 24] and the references listed therein. Studies have also proposed advanced deep learning frameworks for anomaly detection in industrial sensors and for smart contract vulnerability detection [25, 26].

The spread of viruses in WSNs mirrors the transmission dynamics of epidemic diseases in human populations. This analogy has motivated researchers to adopt the well-established frameworks of epidemic modeling to capture the spatial and temporal patterns of the computer virus, evaluate different control strategies, and enhance network resilience in the face of cyber threats [20–22]. While these existing approaches capture key aspects of malware propagation, they often neglect certain features relevant to WSN environments, such as multi-stage exposure, vaccination effects, and stochastic perturbations induced by environmental and operational uncertainties [12]. Keeping in view these aspects, our study advances the epidemic modeling framework by introducing dual exposed compartments, anti-virus administration, and stochastic perturbations in the form of continuous Brownian motion and discontinuous Lévy jump noise terms, thereby enabling a more realistic representation of virus spread and its control in WSNs. The study aims to gain a deeper understanding of the underlying dynamics of computer viruses and reduce malware attacks on these networks. To capture the problem in mathematical terms, we assumed the sensing range of each node as r, and thus, the area under the influence of a virus will be πr^2. Let us denote the susceptible nodes at any time t by the notion $\mathbf{S}(t)$, and thus, the density per unit area is given by $\rho(t) = \frac{\mathbf{S}(t)}{Ł \times Ł}$. Hence, the density of the susceptible nodes within the sensing range is determined by the formula $\mathbf{S}'(t) = \frac{\mathbf{S}(t)\pi r^2}{Ł^2}$. The suggested model increases network longevity and data effectiveness in WSNs. The inclusion of these

features has clear and remarkable outcomes in businesses, especially as they can enhance antivirus systems and efficiently block malware attacks on wireless networks. This study enables users to recover compromised nodes, allowing them to strategically deploy antivirus software on these sensor nodes, thereby enhancing the overall security architecture and minimizing the risk of attacks. This work represents a notable advancement in demonstrating the applicability of the $\mathbf{SE_1E_2IRV}$ model, which may help researchers in gaining a precise understanding of malware spread within WSNs. Our key objective is to investigate the impact of external variables and parameter variability on the dynamic process of worms within the WSN by incorporating white noise perturbations. This study explores how network nodes change and interact within different states, helping to reveal the connections and patterns that link them. Utilizing the principles of stochastic epidemic theory, the $\mathbf{SE_1E_2IRV}$ model is formulated and employed to analyze the spread and control of malware within WSNs. Using different parameter settings, the model was simulated, and the results were provided to validate the analytical results and reveal the complex aspects of the dynamic pattern.

2. Epidemic model of worm spread in wireless sensor network

An epidemic model in the context of a WSNs is often a model that replicates the spread of information, events, or problems between the network nodes. This may be related to data dissemination, the propagation of a specific behavior or condition, or the spread of a malfunction or attack. The epidemic model is frequently used to investigate how rapidly and efficiently information or events may spread across a network. Figure 2 represents a simplified description of an epidemic model flow in a wireless sensor network.

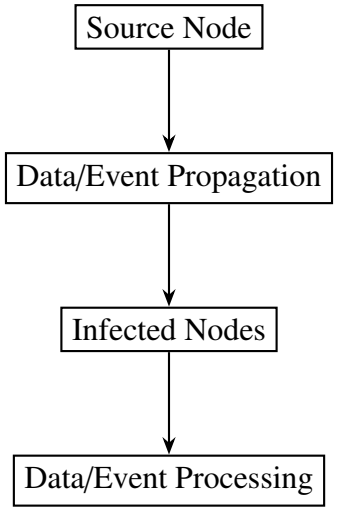

Figure 2. Simplified dynamics of node movement in a wireless sensor network.

Before moving further, let us define and explain a few terminologies of WSNs.

- **Source Node:** The node that initiates the epidemic by generating data, an event, or a fault.
- **Data/Event Propagation:** The process by which information is transmitted from the source node to other nodes in the network. This could be through direct communication, broadcasting, or other methods.

- **Infected Nodes:** Nodes that have received the information or event and are affected by it. In a positive context, this could represent nodes that have successfully received and processed the data. In a negative context, it could represent nodes affected by a fault or attack.
- **Data/Event Processing:** The nodes process the received information or event based on the application requirements.

To develop the governing model, we divided the whole nodes N of the networks into disjoint compartments comprised of six different states, where **S** represents those nodes that are yet not in interaction with the virus but are vulnerable to the malware attack. The modeling framework incorporates two biologically motivated exposed compartments, $\mathbf{E}_1$ and $\mathbf{E}_2$, is motivated by real-world malware propagation patterns observed in wireless sensor networks (WSNs), where different malware strains or attack modes exhibit heterogeneous incubation behaviors. For instance, fast-acting malware that rapidly disrupts node operations is captured by $\mathbf{E}_1$, while stealthy or dormant malware activating later under specific conditions is represented by $\mathbf{E}_2$. This compartmentalization reflects well-documented cybersecurity strategies such as time-delayed activation and layered infection stages, thereby enhancing the biological analogy to diseases with multiple incubation phases. Such a structure improves the model's realism and allows for a more nuanced representation of diverse malware behaviors. The **I** compartment denotes infected sensor nodes capable of propagating malware to neighboring nodes, **R** refers to nodes that have recovered through antivirus measures or other counter-strategies, and **V** represents nodes that have been successfully vaccinated at time t. These total nodes **N** comprise the sub-compartments that are scattered in the area of $Ł^2$. The nodes collect relevant information from the surroundings. As mentioned above, the total nodes are categorized into six groups, namely: vulnerable (**S**), exposed group 1 ($\mathbf{E}_1$), exposed category 1 ($\mathbf{E}_2$), infectious (**I**), recovered (**R**) and (**V**) vaccinated states. Consequently, at each moment $t \geq 0$, the aggregate number of sensor nodes in the network is denoted as $\mathbf{N}(t)$, which adheres to the above requirements:

$$\mathbf{N}(t) = \mathbf{S}(t) + \mathbf{E}_1(t) + \mathbf{E}_2(t) + \mathbf{I}(t) + \mathbf{R}(t) + \mathbf{V}(t). \tag{2.1}$$

The state variables interact within the WSN according to the flowchart diagram presented in Figure 3. The model aims to better understand the dynamic behavior of nodes within the network and to slow down the spread of the virus within the network.

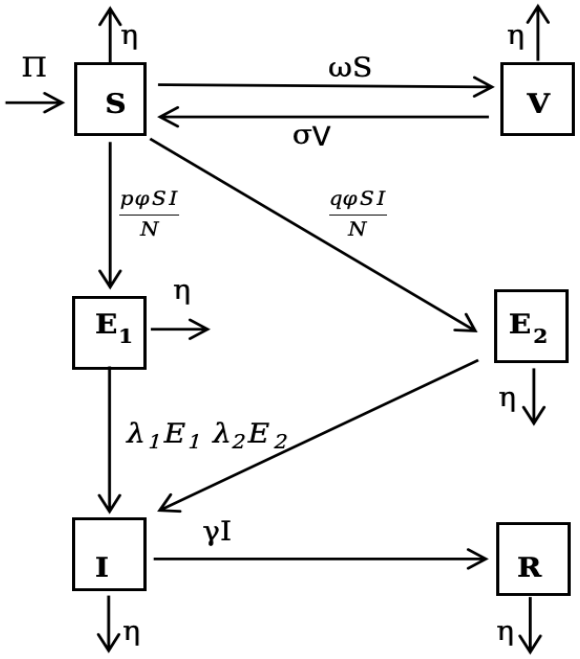

Figure 3. The transfer diagram of a system (2.2).

To formulate the model, we need to utilize the sensing area and susceptibility within the sensing area. Further, for convenience, let $\varphi = \frac{\pi r^2}{\mathrm{L}^2}\beta$. Figure 3 illustrates the evolution of the sensing nodes throughout various stages, as delineated by the subsequent equations:

$$\begin{aligned}
\frac{d\mathbf{S}}{dt} &= \Pi - \frac{\varphi \mathbf{S}(t)\mathbf{I}(t)}{\mathbf{N}(t)} - \eta \mathbf{S}(t) - \omega \mathbf{S}(t) + \sigma \mathbf{V}(t),\\
\frac{d\mathbf{E}_1}{dt} &= \frac{\varphi p \mathbf{I}(t)\mathbf{S}(t)}{\mathbf{N}(t)} - (\lambda_1 + \eta)\,\mathbf{E}_1(t),\\
\frac{d\mathbf{E}_2}{dt} &= \frac{\varphi q \mathbf{S}(t)\mathbf{I}(t)}{\mathbf{N}(t)} - (\eta + \lambda_2)\,\mathbf{E}_2(t),\\
\frac{d\mathbf{I}}{dt} &= \lambda_2 \mathbf{E}_2(t) + \lambda_1 \mathbf{E}_1(t) - (\gamma + \eta)\mathbf{I}(t),\\
\frac{d\mathbf{R}}{dt} &= -\eta \mathbf{R}(t) + \gamma \mathbf{I}(t),\\
\frac{d\mathbf{V}}{dt} &= \omega \mathbf{S}(t) - (\sigma + \eta)\mathbf{V}(t).
\end{aligned} \tag{2.2}$$

The rest of the parameters used in the model are explained in Table 1.

Table 1. Descriptions of the parameters used in system (2.2).

Parameters	Description of parameters
Π	Rate of new node entry into the WSN
η	Crashing rate due to battery depletion
β	Malware spreading rate
p	Proportion entering exposed class $\mathbf{E}_1$
q	Proportion entering exposed class $\mathbf{E}_2$
λ_1, λ_2	Transition rates from exposed to infectious (with $\lambda_1 > \lambda_2$)
γ	Recovery rate
ω	Vaccination rate
σ	Rate of vaccine immunity loss
πr^2	The area of a circular sensing region of a single sensor node

When dealing with real-world situations, the Brownian terms represent continuous stochastic fluctuations in each compartment, capturing effects such as environmental variability, dynamic node behavior, or random communication failures. In contrast, the jump terms $\int_X \alpha_i(y)X(t^-)\,\tilde{P}(d\chi)$, where $i = 1, 2...6$, model rare but impactful shocks such as sudden malware outbreaks or abrupt node crashes through Lévy noise, which realistically accounts for discontinuous events. In real-world WSNs, various unpredictable factors such as node mobility, inconsistent energy usage, communication delays, and hardware instabilities naturally lead to uncertainties. Brownian noise reflects these small-scale, persistent variations, while the jump noise captures infrequent but disruptive events. The choice of α-stable Lévy noise is motivated by the empirical observation that traffic patterns and attack intensities in wireless and computer networks often exhibit heavy-tailed, non-Gaussian fluctuations, where extreme events occur more frequently than predicted by Gaussian models. From a practical perspective, incorporating these stochastic components results in a more realistic and resilient framework for analyzing malware propagation and node dynamics under uncertainty. This formulation enables the quantification of system reliability under random disturbances and provides insights for designing robust control strategies. Furthermore, the noise intensities ξ_i and jump amplitudes $\alpha_i(y)$ serve as tunable parameters that can be estimated from empirical data or adapted to reflect real-world disturbance patterns in WSN environments. The ODEs system (2.2) could be represented in the formalism of stochastic perturbation as follows:

$$
\begin{aligned}
d\mathbf{S} &= \left[\Pi - \frac{\varphi \mathbf{S}(t)\mathbf{I}(t)}{\mathbf{N}(t)} - \eta \mathbf{S}(t) - \omega \mathbf{S}(t) + \sigma \mathbf{V}(t)\right]dt + \xi_1 \mathbf{S}(t) d\mathbf{Q}_1(t) \\
&\quad + \int_X \alpha_1(y)\mathbf{S}(t^-)\tilde{P}(d\chi), \\
d\mathbf{E}_1 &= \left[\frac{p\varphi \mathbf{S}(t)\mathbf{I}(t)}{\mathbf{N}(t)} - (\lambda_1 + \eta)\,\mathbf{E}_1(t)\right]dt + \xi_2 \mathbf{E}_1(t) d\mathbf{Q}_2(t) \\
&\quad + \int_X \alpha_2(y)\mathbf{E}_1(t^-)\tilde{P}(d\chi), \\
d\mathbf{E}_2 &= \left[\frac{q\varphi \mathbf{S}(t)\mathbf{I}(t)}{\mathbf{N}(t)} - (\lambda_2 + \eta)\,\mathbf{E}_2(t)\right]dt + \xi_3 \mathbf{E}_2(t) d\mathbf{Q}_3(t) \\
&\quad + \int_X \alpha_3(y)\mathbf{E}_2(t^-)\tilde{P}(d\chi), \\
d\mathbf{I} &= \left[\lambda_1 \mathbf{E}_1(t) + \lambda_2 \mathbf{E}_2(t) - (\gamma + \eta)\mathbf{I}(t)\right]dt + \xi_4 \mathbf{I}(t) d\mathbf{Q}_4(t) \\
&\quad + \int_X \alpha_4(y)\mathbf{I}(t^-)\tilde{P}(d\chi), \\
d\mathbf{R} &= \left[\gamma \mathbf{I}(t) - \eta \mathbf{R}(t)\right]dt + \xi_5 \mathbf{R}(t) d\mathbf{Q}_5(t) + \int_X \alpha_5(y)\mathbf{R}(t^-)\tilde{P}(d\chi), \\
d\mathbf{V} &= \left[\omega \mathbf{S}(t) - (\sigma + \eta)\mathbf{V}(t)\right]dt + \xi_6 \mathbf{V}(t) d\mathbf{Q}_6(t) + \int_X \alpha_6(y)\mathbf{V}(t^-)\tilde{P}(d\chi),
\end{aligned}
\tag{2.3}
$$

where $(d\chi) = (dt, dx)$.

The terms $\mathbf{Q}_i(t)$, for $i = 1, \ldots, 6$, denote independent standard Brownian motions with $\mathbf{Q}_i(0) = 0$, which are used to model continuous stochastic fluctuations in the system. The coefficients ξ_i represent the intensity of the diffusion noise associated with each corresponding state variable. In addition to these continuous perturbations, the model incorporates discontinuous random effects through the integral terms involving the jump amplitude functions $\alpha_i(y)$ and the compensated Poisson random measure $\tilde{P}(d\chi)$. These terms describe the influence of Lévy jumps, capturing sudden, irregular events such as abrupt node failures or malware bursts. Specifically, $\alpha_i(y)$ defines the size of the jump, while $\tilde{P}(d\chi)$ characterizes the timing and distribution of these stochastic jump events over the space X. Figure 4 illustrates the overall compartmental transitions under the combined influence of both diffusion and jump noise in system (2.3).

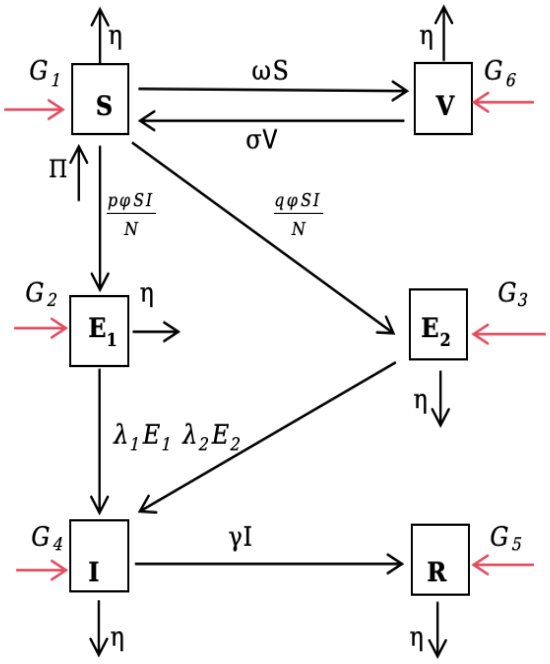

Figure 4. The transfer diagram of a system (2.3).

Let

$$\begin{aligned}
G_1 &= \xi_1 \mathbf{S}(t)d\mathbf{Q}_1(t) + \int_X \alpha_1(y)\mathbf{S}(t^-)\tilde{P}(d\chi),\\
G_2 &= \xi_2 \mathbf{E}_1(t)d\mathbf{Q}_2(t) + \int_X \alpha_2(y)\mathbf{E}_1(t^-)\tilde{P}(d\chi),\\
G_3 &= \xi_3 \mathbf{E}_2(t)d\mathbf{Q}_3(t) + \int_X \alpha_3(y)\mathbf{E}_2(t^-)\tilde{P}(d\chi),\\
G_4 &= \xi_4 \mathbf{I}(t)d\mathbf{Q}_4(t) + \int_X \alpha_4(y)\mathbf{I}(t^-)\tilde{P}(d\chi),\\
G_5 &= \xi_5 \mathbf{R}(t)d\mathbf{Q}_5(t) + \int_X \alpha_5(y)\mathbf{R}(t^-)\tilde{P}(d\chi),\\
G_6 &= \xi_6 \mathbf{V}(t)d\mathbf{Q}_6(t) + \int_X \alpha_6(y)\mathbf{V}(t^-)\tilde{P}(d\chi).
\end{aligned} \tag{2.4}$$

3. Positive solution qualitative analysis

To explain the dynamic behaviors of the model (2.3), it is necessary to demonstrate the existence of a single non-local solution inside the feasible region. Thus, this task can be accomplished effortlessly, and we choose to exclude it. Subsequently, to obtain positive and non-local solutions, it is necessary to employ the methodologies associated with the Lyapunov function [23, 24]. Let us define some

assumptions and lemmas in the stochastic sense.

$$\langle \mathcal{H}(t) \rangle = \frac{1}{t} \int_0^t \mathcal{H}(x) dx.$$

The two standard assumptions, $(\mathbf{H}_1)$ and $(\mathbf{H}_2)$, are essential for proving the existence and uniqueness of a global positive solution to (2.3).

Lemma 1. $(\mathbf{H}_1)$. $\forall\ \mathbf{M} > 0\ \exists\ \mathbb{L}_{\mathbf{M}} > 0$ *such that*

$$\int_{\mathbf{Y}} |\mathbf{Z}_i(y_1, x) - \mathbf{Z}_i(y_2, s)|^2 \nu(dy) \leq \mathbb{L}_{\mathbf{M}} |s_1 - s_2|^2, i = 1, 2, 3, 4, 5, 6, \tag{3.1}$$

with $|s_1| \vee |s_2| \leq \mathbb{M}$, where

$$\begin{aligned}
&\mathbf{Q}_1(s, y) = \Omega_1(y)s \text{ for } s = \mathbf{S}(t^-), \\
&\mathbf{Q}_2(s, y) = \Omega_2(y)s \text{ for } s = \mathbf{E}_1(t^-), \\
&\mathbf{Q}_3(s, y) = \Omega_3(y)s \text{ for } s = \mathbf{E}_2(t^-), \\
&\mathbf{Q}_4(s, y) = \Omega_4(y)s \text{ for } s = \mathbf{I}(t^-), \\
&\mathbf{Q}_5(s, y) = \Omega_5(y)s \text{ for } s = \mathbf{R}(t^-), \\
&\mathbf{Q}_6(s, y) = \Omega_6(y)s \text{ for } s = \mathbf{V}(t^-),
\end{aligned} \tag{3.2}$$

where $\mathbf{Z}$ denotes the compensated random measure.
$(\mathbf{H}_2)$. $\left|\log(1 + \Omega_i(x))\right| \leq C$ for $\Omega_i(s) > -1, \Omega_i = 1, 2, 3, 4, 5, 6$ where C is a positive constant.

Theorem 1. *Assuming an initial set of positive data for the state of variables, a global solution* $(\mathbf{S}, \mathbf{E}_1, \mathbf{E}_2, \mathbf{I}, \mathbf{R}, \mathbf{V})(t) \in \mathbb{R}_+^6$ *exists for all* $0 \leq t$ *in system (*2.3*) a.s.*

Proof. By looking into the coeffecients of model (2.3), we can say that it satisfy the underlying local Lipschitzness, hence the condition $(\mathbf{H}_1)$, for any initial approximations values $(\mathbf{S}_0, \mathbf{E}_1(0), \mathbf{E}_2(0), \mathbf{I}_0, \mathbf{R}_0, \mathbf{V}_0) \in \mathbb{R}_+^6$, it is evident that the coefficients of system (2.3) are locally Lipschitz and continuous. Therefore, a distinct local solution $(\mathbf{S}, \mathbf{E}_1, \mathbf{E}_2, \mathbf{I}, \mathbf{R}, \mathbf{V})(t)$ is present for all values of $t \in [0, \tau_e)$, where τ_e denotes the time of the explosion. To demonstrate that this solution is global, we need to prove that $\tau_e = \infty$ is almost certainly the case. Let $k_0 \geq 0$ be sufficiently large to ensure that the initial values $(\mathbf{S}(0), \mathbf{E}_1(0), \mathbf{E}_2(0), \mathbf{I}(0), \mathbf{R}(0), \mathbf{V}(0))$ lie within the interval $\left[\frac{1}{k_0}, k_0\right]$. We describe the stopping time as follows for each integer $k \geq k_0$:

$$\begin{aligned}
\tau_k = \inf\{t \in [0, \tau_e) : \min(\mathbf{S}(t), \mathbf{E}_1(t), \mathbf{E}_2(t), \mathbf{I}(t), \mathbf{R}(t), \mathbf{V}(t)) \leq \frac{1}{k} \\
\text{or } \max(\mathbf{S}(t), \mathbf{E}_1(t), \mathbf{E}_2(t), \mathbf{I}(t), \mathbf{R}(t), \mathbf{V}(t0)) \geq k\}.
\end{aligned}$$

In this paper, we set $\inf \emptyset = \infty$ (where $\emptyset$ represents the empty set). According to the given definition, τ_k increases as $k \to \infty$. Set $\tau_\infty = \lim_{k \to \infty} \tau_k$, therefore, $\tau_\infty \leq \tau_e$ almost surely. We must demonstrate that $\tau_\infty = \infty$ almost certainly. If this claim is incorrect, then there surely exists a combination of constants $T > 0$ and $\epsilon \in (0, 1)$ that results in

$$P\{\tau_\infty \leq T\} > \epsilon.$$

As a result, there exists a real number $k_0 \leq k_1$ for which

$$P\{T \geq \tau_k\} > \epsilon \quad \forall\, k \geq k_1. \tag{3.3}$$

To continue the proof, assume a function (C^2) $V : \mathbb{R}^5_+ \to \mathbb{R}_+$, where $\mathbb{R}_+ = \{x : x \text{ is real and non-negative}\}$, by

$$\begin{aligned} V(\mathbf{S}, \mathbf{E}_1, \mathbf{E}_2, \mathbf{I}, \mathbf{R}, \mathbf{V}) = (-1 + \mathbf{S} - \ln \mathbf{S}) + (-1 + \mathbf{E}_1 - \ln \mathbf{E}_1) + (-1 + \mathbf{E}_2 - \ln \mathbf{E}_2) + (-1 + \mathbf{I} - \ln \mathbf{I}) \\ + (-1 + \mathbf{R} - \ln \mathbf{R}) + (-1 + \mathbf{V} - \ln \mathbf{V}). \end{aligned}$$

By employing the Itô formula, we derive

$$\begin{aligned} dV = LV\,dt + (\mathbf{S} - 1)\xi_1\,d\mathbf{Q}_1(t) + (\mathbf{E}_1 - 1)\xi_2\,d\mathbf{Q}_2(t) + (\mathbf{E}_2 - 1)\xi_3\,d\mathbf{Q}_3(t) + (\mathbf{I} - 1)\xi_4\,d\mathbf{Q}_4(t) \\ + (\mathbf{R} - 1)\xi_5\,d\mathbf{Q}_5(t) + (\mathbf{V} - 1)\xi_6\,d\mathbf{Q}_6(t) + \int_X [\alpha_1(y)\mathbf{S} - \ln(1 + \alpha_1(y))]\tilde{P}(d\chi) \\ + \int_X [\alpha_2(y)\mathbf{E}_1 - \ln(1 + \alpha_2(y))]\tilde{P}(d\chi) + \int_X [\alpha_3(y)\mathbf{E}_2 - \ln(1 + \alpha_3(y))]\tilde{P}(d\chi) \\ + \int_X [\alpha_4(y)\mathbf{I} - \ln(1 + \alpha_4(y))]\tilde{P}(d\chi) + \int_X [\alpha_5(y)\mathbf{R} - \ln(1 + \alpha_5(y))]\tilde{P}(d\chi) \\ + \int_X [\alpha_6(y)\mathbf{V} - \ln(1 + \alpha_6(y))]\tilde{P}(d\chi). \end{aligned} \tag{3.4}$$

$$\begin{aligned} LV = \left(1 - \frac{1}{\mathbf{S}(t)}\right)\left(\Pi - \frac{\varphi \mathbf{S}(t)\mathbf{I}(t)}{\mathbf{N}(t)} - \eta \mathbf{S}(t) - \omega \mathbf{S}(t) + \sigma \mathbf{V}(t)\right) + \frac{\xi_1^2}{2} \\ + \int_X [\alpha_1(y) - \ln(1 + \alpha_1(y))]\, v(dx) \\ + \left(1 - \frac{1}{\mathbf{E}_1(t)}\right)\left(\frac{p\varphi \mathbf{S}(t)\mathbf{I}(t)}{\mathbf{N}(t)} - (\lambda_1 + \eta)\,\mathbf{E}_1(t)\right) + \frac{\xi_2^2}{2} \\ + \int_X [\alpha_2(y) - \ln(1 + \alpha_2(y))]\, v(dx) \\ + \left(1 - \frac{1}{\mathbf{E}_2(t)}\right)\left(\frac{q\varphi \mathbf{S}(t)\mathbf{I}(t)}{\mathbf{N}(t)} - (\lambda_2 + \eta)\,\mathbf{E}_2(t)\right) + \frac{\xi_3^2}{2} \\ + \int_X [\alpha_3(y) - \ln(1 + \alpha_3(y))]\, v(dx) \\ + \left(1 - \frac{1}{\mathbf{I}(t)}\right)(\lambda_1 \mathbf{E}_1(t) + \lambda_2 \mathbf{E}_2(t) - (\gamma + \eta)\mathbf{I}(t)) + \frac{\xi_4^2}{2} \\ + \int_X [\alpha_4(y) - \ln(1 + \alpha_4(y))]\, v(dx) \\ + \left(1 - \frac{1}{\mathbf{R}(t)}\right)(\gamma \mathbf{I}(t) - \eta \mathbf{R}(t)) + \frac{\xi_5^2}{2} + \int_X [\alpha_5(y) - \ln(1 + \alpha_5(y))]\, v(dx) \\ + \left(1 - \frac{1}{\mathbf{V}(t)}\right)(\sigma + \eta)\mathbf{V}(t)) + \frac{\xi_6^2}{2} + \int_X [\alpha_6(y) - \ln(1 + \alpha_6(y))]\, v(dx). \end{aligned}$$

$$LV \leq \Pi + \varphi + 6\eta + \omega + \lambda_1 + \lambda_2 + \gamma + \sigma + \sum_{i=1}^{6} \frac{\xi_i^2}{2} + \sum_{i=i}^{6} \int_X [\alpha_i(y) - \ln(1 + \alpha_i(y))]v(dx).$$

$$LV \leq \Pi + \varphi + 6\eta + \omega + \lambda_1 + \lambda_2 + \gamma + \sigma + \sum_{i=1}^{6} \frac{\xi_i^2}{2} + \sum_{i=i}^{6} \int_X [\alpha_i(y) - \ln(1 + \alpha_i(y))]v(dx) = \mathbf{K}. \quad (3.5)$$

By integrating both sides of Eq (3.4) within the interval $[0, \alpha_m \wedge T]$, we obtain

$$\begin{aligned} 0 \leq E \quad & \mathbf{S}(\alpha \wedge T),\ \mathbf{E}_1(\alpha \wedge T),\ \mathbf{E}_2(\alpha \wedge T),\ \mathbf{I}(\alpha \wedge T),\ \mathbf{R}(\alpha \wedge T),\ \mathbf{V}(\alpha \wedge T) \\ & \leq H(\mathbf{S}_0, \mathbf{E}_{10}, \mathbf{E}_{20}, \mathbf{I}_0, \mathbf{R}_0, \mathbf{V}_0) + E \int_0^{\alpha \wedge T} \mathbf{K} \\ & \leq H(\mathbf{S}_0, \mathbf{E}_{10}, \mathbf{E}_{20}, \mathbf{I}_0, \mathbf{R}_0, \mathbf{V}_0) + T\mathbf{K}. \end{aligned} \quad (3.6)$$

We reached $P(\alpha) \geq 1$ by supposing $\alpha = \{T \geq \alpha\}$. Next, there exists $(\mathbf{S}(\alpha, \alpha), \mathbf{E}_1(\alpha, \alpha), \mathbf{E}_2(\alpha, \alpha), \mathbf{I}(\alpha, \alpha), \mathbf{R}(\alpha, \alpha), \mathbf{V}(\alpha, \alpha))$ that equal either $\mathbf{K}$ or $\frac{1}{\mathbf{K}}$.

As $H(\mathbf{S}(\alpha), \mathbf{E}_1(\alpha), \mathbf{E}_2(\alpha), \mathbf{I}(\alpha), \mathbf{R}(\alpha), \mathbf{V}(\alpha)) \geq l - \ln l - 1$ or $\frac{1}{l} + \ln l - 1$, so,

$$E(l - \ln l - 1) \wedge (\frac{1}{l} + \ln l - 1) \leq H(\mathbf{S}_{\alpha_l}, \mathbf{E}_{1\alpha_l}, \mathbf{E}_{2\alpha_l}, \mathbf{I}_{\alpha_l}, \mathbf{R}_{\alpha_l}, \mathbf{V}_{\alpha_l}). \quad (3.7)$$

As $0 < P(T > \omega+)$ and with the use of Eq (3.6), we have

$$\begin{aligned} H(\mathbf{S}_0, \mathbf{E}_{10}, \mathbf{E}_{20}, \mathbf{I}_0, \mathbf{R}_0, \mathbf{V}_0) + \mathbf{K}T & \geq E\left[1_{\Omega_{(\omega)}} H(\mathbf{S}_{\alpha_l}, \mathbf{E}_{1\alpha_l}, \mathbf{E}_{2\alpha_l}, \mathbf{I}_{\alpha_l}, \mathbf{R}_{\alpha_l}, \mathbf{V}_{\alpha_l})\right] \\ & \geq \epsilon\left[(l - \ln l - 1) \wedge (\frac{1}{l} + \ln l - 1)\right]. \end{aligned} \quad (3.8)$$

Here $1_{\Omega_{(\omega)}}$ denotes the set Ω. Substituting l with ∞ results in a contradiction: $\infty > H(\mathbf{S}_0, \mathbf{E}_{10}, \mathbf{E}_{20}, \mathbf{I}_0, \mathbf{R}_0, \mathbf{V}_0) + \mathbf{K}T = \infty$. Consequently, the system exhibits exceptional well-posedness. □

4. Extinction

The objective of this section is to analyze the extinction of the system (2.3) and establish a threshold for assessing the likelihood of the worm's eventual extinction or survival. We will determine the circumstances that will lead to the eradication of a worm. To facilitate comprehension, it is necessary to establish a clear and concise definition.

Lemma 2. *If in model (2.3),* $(\mathbf{S}, \mathbf{E}_1, \mathbf{E}_2, \mathbf{I}, \mathbf{R}, \mathbf{V})$ *is a root with starting approximation*

$$(\mathbf{S}(0), \mathbf{E}_1(0), \mathbf{E}_2(0), \mathbf{I}(0), \mathbf{R}(0), \mathbf{V}(0)) \in \mathbb{R}_+^6,$$

then a.s.,

$$\lim_{t \to \infty} \frac{\mathbf{S}(t) + \mathbf{E}_1(t) + \mathbf{I}(t) + \mathbf{E}_2(t) + \mathbf{R}(t) + \mathbf{V}(t)}{t} = 0. \quad (4.1)$$

Further,

$$\lim_{t \to \infty} \frac{1}{t} \int_0^t \mathbf{S}(r)\, dQ_1(r) = 0, \quad \lim_{t \to \infty} \frac{1}{t} \int_0^t \mathbf{E}_1(r)\, dQ_2(r) = 0, \quad \lim_{t \to \infty} \frac{1}{t} \int_0^t \mathbf{E}_2(r)\, dQ_3(r) = 0,$$

$$\lim_{t\to\infty}\frac{1}{t}\int_0^t \mathbf{I}(r)\,dQ_4(r)=0,\quad \lim_{t\to\infty}\frac{1}{t}\int_0^t \mathbf{R}(r)\,dQ_5(r)=0,\quad \lim_{t\to\infty}\frac{1}{t}\int_0^t \mathbf{R}(r)\,dQ_5(r)=0.$$

Proof. The mathematical calculation of the aforementioned result is removed, since the final remarks may be derived using the methodology outlined in the formulation of Lemma 4.1 in Zhang et al. [27]. □

Theorem 2. *If the threshold number*

$$\mathbf{R_0^S}=\frac{\phi\left[\lambda_1\lambda_2+\eta(p\lambda_1+q\lambda_2)\right]}{(\eta+\gamma)(\lambda_1\lambda_2+\eta\lambda_1+\eta\lambda_2+\eta^2)+\frac{\xi^2}{4}+\int_X\left[\alpha_4(y)+\ln(1+\alpha_4(y))\right]\mu dy}<1,$$

then the infected nodes $\mathbf{I}(t)$ in system (2.3) will almost certainly approach zero as a result of an exponential function.

Proof. By integrating the model (2.3), we can get the below outlined equations:

$$\begin{aligned}
\frac{\mathbf{S}(t)-\mathbf{S}(0)}{t}&=\Pi-\frac{\phi\langle\mathbf{S}\rangle\langle\mathbf{I}\rangle}{\langle\mathbf{N}\rangle}-\eta\langle\mathbf{S}\rangle-\omega\langle\mathbf{S}\rangle+\sigma\langle\mathbf{V}\rangle+\frac{\xi_1}{t}\int_0^t\mathbf{S}(t)\,dQ_1(t)\\
&\quad+\frac{1}{t}\int_0^t\left[\int_X\alpha_1(y)\mathbf{S}(t^-)\tilde{P}(d\chi)\right],\\
\frac{\mathbf{E}_1(t)-\mathbf{E}_1(0)}{t}&=\frac{p\phi\langle\mathbf{S}\rangle\langle\mathbf{I}\rangle}{\langle\mathbf{N}\rangle}-(\lambda_1+\eta)\langle\mathbf{E}_1\rangle+\frac{\xi_2}{t}\int_0^t\mathbf{E}_1(t)\,dQ_2(t)\\
&\quad+\frac{1}{t}\int_0^t\left[\int_X\alpha_2(y)\mathbf{E}_1(t^-)\tilde{P}(d\chi)\right],\\
\frac{\mathbf{E}_2(t)-\mathbf{E}_2(0)}{t}&=\frac{q\phi\langle\mathbf{S}\rangle\langle\mathbf{I}\rangle}{\langle\mathbf{N}\rangle}-(\lambda_2+\eta)\langle\mathbf{E}_2\rangle+\frac{\xi_3}{t}\int_0^t\mathbf{E}_2(t)\,dQ_3(t)\\
&\quad+\frac{1}{t}\int_0^t\left[\int_X\alpha_3(y)\mathbf{E}_2(t^-)\tilde{P}(d\chi)\right],\\
\frac{\mathbf{I}(t)-\mathbf{I}(0)}{t}&=\lambda_1\langle\mathbf{E}_1\rangle+\lambda_2\langle\mathbf{E}_2\rangle-(\eta+\gamma)\langle\mathbf{I}\rangle+\frac{\xi_4}{t}\int_0^t\mathbf{I}(t)\,dQ_4(t)\\
&\quad+\frac{1}{t}\int_0^t\left[\int_X\alpha_4(y)\mathbf{I}(t^-)\tilde{P}(d\chi)\right],\\
\frac{\mathbf{R}(t)-\mathbf{R}(0)}{t}&=\gamma\langle\mathbf{I}\rangle-\eta\langle\mathbf{R}\rangle+\omega\langle\mathbf{S}\rangle+\frac{\xi_5}{t}\int_0^t\mathbf{R}(t)\,dQ_5(t)\\
&\quad+\frac{1}{t}\int_0^t\left[\int_X\alpha_5(y)\mathbf{I}(t^-)\tilde{P}(d\chi)\right],\\
\frac{\mathbf{V}(t)-\mathbf{V}(0)}{t}&=\omega\langle\mathbf{S}\rangle-(\sigma+\eta)\langle\mathbf{V}\rangle+\frac{\xi_6}{t}\int_0^t\mathbf{V}(t)\,dQ_6(t)\\
&\quad+\frac{1}{t}\int_0^t\left[\int_X\alpha_6(y)\mathbf{V}(t^-)\tilde{P}(d\chi)\right].
\end{aligned}\tag{4.2}$$

Let

$$P(t)=\lambda_1(\lambda_2+\eta)\mathbf{E}_1+\lambda_2(\lambda_1+\eta)\mathbf{E}_2+(\lambda_1+\eta)(\lambda_2+\eta)\mathbf{I}.$$

After simplification, we have:

$$P(t) = \frac{\lambda_1\lambda_2\phi\mathbf{SI}}{\mathbf{N}} + \frac{\eta\phi\mathbf{SI}}{\mathbf{N}}(\lambda_1 p + \lambda_2 q) - (\eta+\gamma)(\lambda_1\lambda_2 + \lambda_1\eta + \lambda_2\eta + \eta^2)\mathbf{I}. \tag{4.3}$$

By the Itô formula, one can get:

$$\begin{aligned}
d\ln\mathbf{I}(t) &= \left[\frac{\lambda_1\lambda_2\phi\mathbf{SI}}{\mathbf{N}} + \frac{\phi\mathbf{SI}}{\mathbf{N}}(\lambda_1 p + \lambda_2 q)\eta - (\eta+\gamma)(\lambda_1\lambda_2 + \lambda_1\eta + \lambda_2\eta + \eta^2)\mathbf{I}\right]\frac{1}{\mathbf{I}}dt \\
&\quad - \frac{\xi_4^2}{2}dt + \xi_4 dQ_4 + \frac{1}{t}\int_X [\ln(1+\alpha_4(y))]\,\tilde{P}(d\chi) - \int_X [\alpha_4(y) - \ln(1+\alpha_4(y))]\,\mu dy, \\
&\leq [\phi(\lambda_1\lambda_2 + \eta(\lambda_1 p + \lambda_2 q)) - ((\eta+\gamma)(\lambda_1\lambda_2 + \lambda_1\eta + \lambda_2\eta + \eta^2) \\
&\quad + \frac{\xi_2^2}{4}\int_X [\alpha_4(y) - \ln(1+\alpha_4(y))]\mu dy)]dt + \xi_4 dQ_4 + \frac{1}{t}\int_X [\ln(1+\alpha_4(y))]\mu dy, \\
&\leq \left[(\eta+\gamma)(\lambda_1\lambda_2 + \eta\lambda_1 + \eta\lambda_2 + \eta^2) + \frac{\xi^2}{4} + \int_X [\alpha_4(y) + \ln(1+\alpha_4(y))]\,\mu dy\right] \\
&\quad \left[\frac{\phi\,[\lambda_1\lambda_2 + \eta(p\lambda_1 + q\lambda_2)]}{(\eta+\gamma)(\lambda_1\lambda_2 + \eta\lambda_1 + \eta\lambda_2 + \eta^2) + \frac{\xi^2}{4} + \int_X [\alpha_4(y) + \ln(1+\alpha_4(y))]\,\mu dy} - 1\right]dt \\
&\quad + \alpha_4 dQ_4 + \frac{1}{t}\int_X [\ln(1+\alpha_4(y))\tilde{P}(d\chi) \\
&\leq \left[(\eta+\gamma)(\lambda_1\lambda_2 + \eta\lambda_1 + \eta\lambda_2 + \eta^2) + \frac{\xi^2}{4} + \int_X [\alpha_4(y) + \ln(1+\alpha_4(y))]\,\mu dy\right]\left[\mathbf{R_0^S} - 1\right]dt \\
&\quad + \alpha_4 dQ_4 + \frac{1}{t}\int_X [\ln(1+\alpha_4(y))\tilde{P}(d\chi)
\end{aligned} \tag{4.4}$$

Integrating system (2.3) throughout the interval 0 to t and using Lemma 2, we obtain:

$$\limsup_{t\to\infty}\frac{\ln\mathbf{I}(t)}{t} \leq \left[(\eta+\gamma)(\lambda_1\lambda_2 + \eta\lambda_1 + \eta\lambda_2 + \eta^2) + \frac{\xi^2}{4} + \int_X [\alpha_4(y) + \ln(1+\alpha_4(y))]\,\mu dy\right]\left[\mathbf{R_0^S} - 1\right], \tag{4.5}$$

which shows that

$$\lim_{t\to\infty}\mathbf{I}(t) = 0. \tag{4.6}$$

In the view of the above-given result, our (4.2) equations satisfy:

$$\frac{\mathbf{R}(t) - \mathbf{R}(0)}{t} = \lambda_1\langle\mathbf{E}_1\rangle + \lambda_2\langle\mathbf{E}_2\rangle - (\eta+\gamma)\langle\mathbf{I}\rangle + \frac{\xi_4}{2}\int_0^t \mathbf{I}(t)\,dQ_4(t) + \frac{1}{t}\int_0^t\left[\int_X \alpha_5(y)\mathbf{I}(t^-)\tilde{P}(d\chi)\right].$$

Applying limits with respect to $t\to\infty$, we can have:

$$\begin{aligned}
\lim_{t\to\infty}\frac{\mathbf{R}(t) - \mathbf{R}(0)}{t} &= \lambda_1\lim_{t\to\infty}\langle\mathbf{E}_1\rangle + \lambda_2\lim_{t\to\infty}\langle\mathbf{E}_2\rangle - (\eta+\gamma)\lim_{t\to\infty}\langle\mathbf{I}\rangle + \frac{\xi_4}{2}\lim_{t\to\infty}\int_0^t \mathbf{I}(t)\,dQ_4(t) \\
&\quad + \frac{1}{t}\lim_{t\to\infty}\int_0^t\left[\int_X \alpha_5(y)\mathbf{I}(t^-)\tilde{P}(d\chi)\right].
\end{aligned}$$

According to Lemma 2, and the above result, we can get:

$$\lim_{t\to\infty} \mathbf{R}(t) = 0,$$

and the rest of the equations of (4.2) are given as:

$$\lim_{t\to\infty} \mathbf{S}(t) = \frac{\Pi}{\eta + \omega - \frac{\sigma(\sigma+\eta)}{\omega}},$$

$$\lim_{t\to\infty} \mathbf{V}(t) = \frac{\Pi(\sigma+\eta)}{\omega(\eta + \omega - \frac{\omega}{\sigma(\sigma+\eta)})}.$$

This explain the asymptotic behavior of the stochastic system (2.3). Thus, the Theorem 2 fundamental objective remains valid. □

5. Persistence

This section examines the long-term dynamics of the illness and its fluctuating effects throughout time. We will begin this process by defining the concept of persistence for the specified average metric. This fundamental phase will help in understanding how the disease persists within the community over prolonged periods.

Definition 1. *Liu and Aeshah [23] presented the following hypothesis to tackle the continued existence or upkeep of the system (2.3):* $\liminf_{t\to\infty} \frac{1}{t}\int_0^t \mathbf{I}(r)dr > 0$ *a.s.*

This assumption indicates the requirement for the disease's sustained presence inside the system throughout time.

Furthermore, confirming epidemic persistence may necessitate essential findings presented by El Fatini and Sekkak [28]. These results are crucial instruments for achieving a thorough comprehension of epidemic dynamics within the specified context.

Lemma 3. *((Strong Law) [28, 29]), If a function which is continuous* $F = \{F\}_{0\leq t}$*, exist at a local martingale such that at* $t \to 0$ *it dies, then*

$$\lim_{t\to\infty}\langle F,F\rangle_t = \infty, \text{ a.s., } \Rightarrow \lim_{t\to\infty}\frac{F_t}{\langle F,F\rangle_t} = 0, \quad a.s.$$

$$\limsup_{t\to\infty}\frac{\langle F,F\rangle_t}{t} < 0, a.s., \Rightarrow \lim_{t\to\infty}\frac{F_t}{t} = 0, \quad a.s.$$

Lemma 4. *Consider* $h \in C([0,\infty)\times\Omega,(0,\infty))$ *and* $\mathbf{H} \in C([0,\infty)\times\Omega,\mathbb{R}) \ni \lim_{t\to\infty}\frac{\mathbf{H}(t)}{t} = 0$ *a.s. If for all* $t \geq 0$, $\ln h(t) \geq \xi_0 t - \xi\int_0^t h(s)ds + \mathbf{H}(t)$ *a.s., then,* $\liminf_{t\to\infty}\langle h(t)\rangle \geq \frac{\Xi_0}{\Xi}$ *a.s., where* $\{\Xi,\Xi_0 \in R \ni \Xi > 0$ G $\Xi_0 \geq 0\}$*. The following theorem will outline the assumptions pertaining to the permanence of the system (2.3). The primary purpose of this section is explained in the subsequent theorem, which delineates the formal requirements for persistence.*

Theorem 3. *If* $\mathbf{R_0^P} > 1$*, with initial data* $(\mathbf{S}_0,\mathbf{E}_1(0),\mathbf{E}_2(0),\mathbf{I}_0,\mathbf{R}_0,\mathbf{V}_0) \in \mathbb{R}^6_+$*, the worm* $\mathbf{I}(t)$ *will be subject to the following condition:*

$$\liminf_{t\to\infty}\langle \mathbf{I}(t)\rangle \geq \frac{4\Pi\left(\sqrt{\mathbf{R_0^P}} - 1\right)}{C_1\varphi} \quad a.s.$$

where

$$C_1 = \frac{\Pi}{\left(\eta + \omega + \frac{\xi_1^2}{2} + \int_X [\alpha_1(y) - \ln(1 + \alpha_1(y))]\,\mu(dy)\right)}.$$

Consequently, we may assert that the malware will persist throughout the network. Let us stated

$$\mathbf{R_0^P} = \frac{pq\varphi^2\lambda_1}{\left(\eta + \omega + \frac{\xi_1^2}{2} + A_1\right)\left(\lambda_1 + \eta + \frac{\xi_2^2}{2} + A_2\right)\left(\lambda_2 + \eta + \frac{\xi_3^2}{2} + A_3\right)\left(\gamma + \eta + \frac{\xi_4^2}{2} + A_4\right)},$$

where

$$A_1 = \int_X [\alpha_1(y) - \ln(1 + \alpha_1(y))]\,\mu(dy).$$

$$A_2 = \int_X [\alpha_2(y) - \ln(1 + \alpha_2(y))]\,\mu(dy).$$

$$A_3 = \int_X [\alpha_3(y) - \ln(1 + \alpha_3(y))]\,\mu(dy).$$

$$A_4 = \int_X [\alpha_4(y) - \ln(1 + \alpha_4(y))]\,\mu(dy).$$

Proof. Set

$$G = -C_1 \ln \mathbf{S} - C_2 \ln \mathbf{E}_1 - C_3 \ln \mathbf{E}_2 - C_4 \ln \mathbf{I}, \tag{5.1}$$

here C_1, C_2, C_3, and C_4 are contants, and we may calculate it later. By the application of Itô result on Eq (5.1), we get

$$\begin{aligned} dG = {} & LG - C_1\xi_1 dQ_1(t) - C_2 dQ_2(t) - C_3 dQ_3(t) - C_4 dQ_4(t) \\ & - C_1 \int_X [\alpha_1 \mathbf{S} - \ln(1 + \alpha_1)]\,\tilde{N}(dt, dx) - C_2 \int_X [\alpha_2 \mathbf{E}_1 - \ln(1 + \alpha_2)]\,\tilde{P}(d\chi) \\ & - C_3 \int_X [\alpha_3 \mathbf{E}_2 - \ln(1 + \alpha_3)]\,\tilde{N}(dt, dx) - C_4 \int_X [\alpha_4 \mathbf{I} - \ln(1 + \alpha_4)]\,\tilde{P}(d\chi), \end{aligned}$$

$$dG = -C_1 \ln \mathbf{S} - C_2 \ln \mathbf{E}_1 - C_3 \ln \mathbf{E}_2 - C_4 \ln \mathbf{I},$$

$$\begin{aligned} dG = {} & -\frac{C_1\Pi}{\mathbf{S}} + \frac{C_1\varphi\mathbf{I}}{\mathbf{N}} + C_1(\eta + \omega) - \frac{C_3\sigma\mathbf{V}}{\mathbf{S}} + \frac{C_1\xi_1^2}{2} + C_1\{\int_X [\alpha_1(y) - \ln(1 + \alpha_1(y))\mu dy]\} \\ & - \frac{C_2 p\varphi\mathbf{S}}{\mathbf{E}_1} + C_2(\lambda_1 + \eta) + \frac{C_2\xi_2^2}{2} + C_2\{\int_X [\alpha_2(y) - \ln(1 + \alpha_2(y))\mu dy]\} \\ & - \frac{C_3 q\varphi\mathbf{SI}}{\mathbf{N}} + C_3(\lambda_2 + \eta) + \frac{C_3\xi_3^2}{2} + C_3\{\int_X [\alpha_3(y) - \ln(1 + \alpha_3(y))\mu dy]\} \\ & - \frac{C_4\lambda_1\mathbf{E}_1}{\mathbf{I}} - \frac{C_4\lambda_2\mathbf{E}_2}{\mathbf{I}} + \frac{C_4\xi_4^2}{2} + C_4\{\int_X [\alpha_4(y) - \ln(1 + \alpha_4(y))\mu dy]\}. \end{aligned}$$

$$dG \leq \left(-\frac{C_1\Pi}{\mathbf{S}} - \frac{C_2 p\varphi\mathbf{S}}{\mathbf{E}_1} - C_3 q\varphi\mathbf{I} - \frac{C_4\lambda_1\mathbf{E}_1}{\mathbf{I}}\right) + C_1\{\frac{\xi_1^2}{2} + \int_X [\alpha_1(y) - \ln(1+\alpha_1(y))\mu dy]\}$$
$$+ C_2\{\frac{\xi_2^2}{2} + \int_X [\alpha_2(y) - \ln(1+\alpha_2(y))\mu dy]\} + C_3\{\frac{\xi_3^2}{2} + \int_X [\alpha_3(y) - \ln(1+\alpha_3(y))\mu dy]\}$$
$$+ C_4\{\frac{\xi_4^2}{2} + \int_X [\alpha_4(y) - \ln(1+\alpha_4(y))\mu dy]\} + C_1\varphi\mathbf{I}.$$

$$dG \leq \sqrt[4]{C_1C_2C_3C_4pq\varphi^2\lambda_1} + C_1\{\frac{\xi_1^2}{2} + \int_X [\alpha_1(y) - \ln(1+\alpha_1(y))\mu dy]\}$$
$$+ C_2\{\frac{\xi_2^2}{2} + \int_X [\alpha_2(y) - \ln(1+\alpha_2(y))\mu dy]\} + C_3\{\frac{\xi_3^2}{2} + \int_X [\alpha_3(y) - \ln(1+\alpha_3(y))\mu dy]\}$$
$$+ C_4\{\frac{\xi_4^2}{2} + \int_X [\alpha_4(y) - \ln(1+\alpha_4(y))\mu dy]\} + C_1\varphi\mathbf{I},$$

where

$$C_1 = \frac{\Pi}{\eta + \omega + \frac{\xi_1^2}{2} + \int_X [\alpha_1(y) - \ln(1+\alpha_1(y))]\mu dy},$$
$$C_2 = \frac{\Pi}{\lambda_1 + \eta + \frac{\xi_2^2}{2} + \int_X [\alpha_2(y) - \ln(1+\alpha_2(y))]\mu dy},$$
$$C_3 = \frac{\Pi}{\lambda_2 + \eta + \frac{\xi_3^2}{2} + \int_X [\alpha_3(y) - \ln(1+\alpha_3(y))]\mu dy},$$
$$C_4 = \frac{\Pi}{\gamma + \eta + \frac{\xi_4^2}{2} + \int_X [\alpha_4(y) - \ln(1+\alpha_4(y))]\mu dy}.$$

Also, we have

$$a = \eta + \omega + \frac{\xi_1^2}{2} + \int_X [\alpha_1(y) - \ln(1+\alpha_1(y))]\mu dy,$$
$$b = \lambda_1 + \eta + \frac{\xi_2^2}{2} + \int_X [\alpha_2(y) - \ln(1+\alpha_2(y))]\mu dy,$$
$$c = \lambda_2 + \eta + \frac{\xi_3^2}{2} + \int_X [\alpha_3(y) - \ln(1+\alpha_3(y))]\mu dy,$$
$$d = \gamma + \eta + \frac{\xi_4^2}{2} + \int_X [\alpha_4(y) - \ln(1+\alpha_4(y))]\mu dy.$$

Then

$$\begin{aligned} LG &\leq -4\sqrt[4]{\frac{\Pi^4 pq\varphi^2\lambda_1}{abcd}} + 4\Pi + C_1\varphi\mathbf{I}, \\ &\leq -4\Pi\left[\sqrt[4]{\frac{pq\varphi^2\lambda_1}{abcd}} - 1\right] + C_1\varphi\mathbf{I}, \\ &\leq -4\Pi\left[\sqrt[4]{\mathbf{R}_0^P} - 1\right] + C_1\varphi\mathbf{I}. \end{aligned} \tag{5.2}$$

Placing Eq (5.2) in Eq (5.1), then taking the integral on both sides, we have

$$\begin{aligned}\frac{G(\mathbf{S}(t),\mathbf{E}_1(t),\mathbf{E}_2(t),\mathbf{I}(t))-\mathbf{S}(0),\mathbf{E}_1(0),\mathbf{E}_2(0),\mathbf{I}(0))}{t} &\leq -4\Pi\Big[\sqrt[4]{\mathbf{R}_0^P}-1\Big]+C_1\varphi\mathbf{I}-\frac{C_1\xi_1^2Q_1(t)}{t}\\ &-\frac{C_2\xi_2^2Q_2(t)}{t}-\frac{C_3\xi_3^2Q_3(t)}{t}-\frac{C_4\xi_4^2Q_4(t)}{t}\\ &-C_1\int_X[\alpha_1(y)\mathbf{S}-\ln(1+\alpha_1(y))]\tilde{N}(d\chi)\\ &-C_2\int_X[\alpha_2(y)\mathbf{E}_1-\ln(1+\alpha_2(y))]\tilde{N}(d\chi)\\ &-C_3\int_X[\alpha_3(y)\mathbf{E}_2-\ln(1+\alpha_3(y))]\tilde{N}(d\chi)\\ &-C_4\int_X[\alpha_4(y)\mathbf{I}-\ln(1+\alpha_4(y))]\tilde{N}(d\chi).\end{aligned} \tag{5.3}$$

We have

$$\begin{aligned}\Psi(t)=&-\frac{C_1\xi_1^2Q_1(t)}{t}-\frac{C_2\xi_2^2Q_2(t)}{t}-\frac{C_3\xi_3^2Q_3(t)}{t}-\frac{C_4\xi_4^2Q_4(t)}{t}-C_1\int_X[\alpha_1(y)\mathbf{S}-\ln(1+\alpha_1(y))]\tilde{N}(d\chi)\\ &-C_2\int_X[\alpha_2(y)\mathbf{E}_1-\ln(1+\alpha_2(y))]\tilde{N}(d\chi)-C_3\int_X[\alpha_3(y)\mathbf{E}_2-\ln(1+\alpha_3(y))]\tilde{N}(d\chi)\\ &-C_4\int_X[\alpha_4(y)\mathbf{I}-\ln(1+\alpha_4(y))]\tilde{N}(d\chi).\end{aligned}$$

From the robust law articulated in Lemma 3, we derive

$$\lim_{t\to\infty}\Psi(t)=0.$$

From Eq (5.3), we have

$$C_1\varphi\langle\mathbf{I}\rangle\geq 4\Pi(\sqrt[4]{\mathbf{R}_0^P}-1)-\Psi(t)+\frac{G(\mathbf{S}(t),\mathbf{E}_1(t),\mathbf{E}_2(t),\mathbf{I}(t))-\mathbf{S}(0),\mathbf{E}_1(0),\mathbf{E}_2(0),\mathbf{I}(0))}{t}. \tag{5.4}$$

By Lemma 4, the limit superior of the equation $\lim_{t\to\infty}\Psi(t)=0$, we have

$$\liminf_{t\to\infty}\langle\mathbf{I}(t)\rangle\geq\frac{4\Pi(\sqrt[4]{\mathbf{R}_0^P}-1)}{C_1\varphi}\quad a.s.$$

thus implies that $\lim_{t\to\infty}\mathbf{I}(t)\geq 0$.
Thus, the proof of Theorem 3 is finished. □

6. Numerical simulations

To handle these dynamics, an extended Milstein scheme is often used, which incorporates corrections to address the jump components introduced by Lévy noise [28]. Lévy-driven stochastic differential equations (SDEs) provide mathematical models for systems influenced by random fluctuations that exhibit abrupt changes, such as in finance, biology, and physics. The extended Milstein technique incorporates both the continuous Gaussian components and the discontinuous jump terms, enhancing the accuracy of simulations compared to simpler schemes like the Euler-Maruyama.

The Milstein scheme for a one-dimensional SDE driven byLévy noise can be described as follows:

$$\mathbf{X}_{n+1} = \mathbf{X}_n + b(\mathbf{X}_n, t_n)\Delta\mathbf{Q}_n + a(\mathbf{X}_n, t_n)\Delta t + \int_{\mathbf{R}} c(\mathbf{X}_n, t_n, \zeta)\Delta\tilde{\mathbf{N}}(\zeta, t_n), \tag{6.1}$$

where:

- $(\mathbf{X}_n)$ represents the value of the process at time t_n.
- $(a(\mathbf{X}_n, t_n))$ and $(b(\mathbf{X}_n, t_n))$ are the drift and diffusion coefficients in the SDE.
- Δt is the time step.
- $(\Delta\mathbf{Q}_n)$ is the increment of the Wiener process (Brownian motion) at time t_n.
- $(c(\mathbf{X}_n, t_n, \zeta))$ is the jump amplitude function, depending on the jump size ζ.
- $(\Delta\tilde{\mathbf{N}}(\zeta, t_n))$ represents the compensated Poisson jump increments associated with the Lévy process.

The extended Milstein scheme incorporates both small and large jumps to ensure that the simulation captures the essential characteristics of Lévy noise. The integral term accounts for the effect of discontinuous jumps, which are modeled using a Poisson random measure or its compensated version. This makes the method particularly suitable for systems where jump discontinuities have significant impacts on the dynamics. This section of the manuscript includes an example, which will subsequently be utilized to simulate the model and demonstrate its behavior of the model. Particularly, the section focuses on the development and implementation of the method and its comparison with other known methods. We shall apply the usual higher-order Milstein technique to the discretized system (2.3). The corresponding discretization equations are provided as follows:

$$
\begin{aligned}
\mathbf{S}_{i+1} &= \mathbf{S}_i + \left[\Pi - \frac{\varphi \mathbf{S}_i \mathbf{I}_i}{\mathbf{N}_i} - \eta \mathbf{S}_i - \omega \mathbf{S}_i + \sigma \mathbf{V}_i\right] \triangle\, t + \xi_1 \mathbf{S}_i \sqrt{\triangle t}\alpha_{1,i} + \frac{\xi_1^2}{2}\mathbf{S}_i(\alpha_{1,i}^2 - 1) \triangle\, t + e(x^*)\mathbf{S}^n \Delta \mathbb{L}_n,\\
\mathbf{E}_{1,i+1} &= \mathbf{E}_{1,i} + \left[\frac{p\varphi \mathbf{S}_i \mathbf{I}_i}{\mathbf{N}_i} - (\lambda_1 + \eta)\,\mathbf{E}_{1,i}\right] \triangle\, t + \xi_2 \mathbf{E}_1 \sqrt{\triangle t}\alpha_{2,i} + \frac{\xi_2^2}{2}\mathbf{E}_{1,i}(\alpha_{2,i}^2 - 1) \triangle\, t + e(x^*)\mathbf{E}_1^n \Delta \mathbb{L}_n,\\
\mathbf{E}_{2,i+1} &= \mathbf{E}_{2,i} + \left[\frac{q\varphi \mathbf{S}_i \mathbf{I}_i}{\mathbf{N}_i} - (\lambda_2 + \eta)\,\mathbf{E}_{2,i}\right] \triangle\, t + \xi_3 \mathbf{E}_2 \sqrt{\triangle t}\alpha_{3,i} + \frac{\xi_3^2}{2}\mathbf{E}_{2,i}(\alpha_{3,i}^2 - 1) \triangle\, t + e(x^*)\mathbf{E}_2^n \Delta \mathbb{L}_n,\\
\mathbf{I}_{i+1} &= \mathbf{I}_i + \left[\lambda_1 \mathbf{E}_{1,i} + \lambda_2 \mathbf{E}_{2,i} - (\gamma + \eta)\mathbf{I}_i\right] \triangle\, t + \xi_4 \mathbf{I} \sqrt{\triangle t}\alpha_{4,i} + \frac{\xi_4^2}{2} I_i(\alpha_{4,i}^2 - 1) \triangle\, t + e(x^*)\mathbf{I}^n \Delta \mathbb{L}_n,\\
\mathbf{R}_{i+1} &= \mathbf{R}_i + \left[\gamma \mathbf{I}_i - \eta \mathbf{R}_i\right] \triangle\, t + \xi_5 \mathbf{R}_i \sqrt{\triangle t}\alpha_{5,i} + \frac{\xi_5^2}{2}\mathbf{R}_i(\alpha_{5,i}^2 - 1) \triangle\, t + e(x^*)\mathbf{R}^n \Delta \mathbb{L}_n,\\
\mathbf{V}_{i+1} &= \mathbf{V}_i + \left[\mathbf{S}_i - (\sigma + \eta)\mathbf{V}_i\right] \triangle\, t + \xi_6 \mathbf{V}_i \sqrt{\triangle t}\alpha_{6,i} + \frac{\xi_6^2}{2}\mathbf{V}_i(\alpha_{6,i}^2 - 1) \triangle\, t + e(x^*)\mathbf{V}^n \Delta \mathbb{L}_n.
\end{aligned}
\tag{6.2}
$$

In the aforementioned context, the notion Δt denotes a positive, uniform time increment. The parameters α_i, for $i = 1, \ldots, 5$, are independent Gaussian stochastic variables, each adhering to the conventional Gaussian distribution $\mathcal{N}(0, 1)$. The simulation period is established as $[0, 5000]$, with a step size of $\Delta t = 0.5$.

6.1. Extinction of the worms

It is commonly noticed from the dynamical analysis that for the threshold value less than one, the number of infected nodes approaches zero. The numerical verification shown above gives empirical evidence confirming the assumption of worm extinction, namely that the worm gradually and consistently disappears from the network when the threshold value is less than one. Figures 5(a)–5(f), obtained from the original experiment, support the aforementioned observation. Table 2 (Case 1) presents the system's parameters and initial settings associated with simulating the system (2.3), where $\mathbf{R}_0^{\mathbf{S}} \approx 0.0169$ if $\alpha_4(y) = 0.1$, and it is integrated over a unit measure (i.e., $\int_X dy = 1$). Furthermore, the stochastic curves obtained from the model (2.3) show variations and finally converge towards the worm-free equilibrium point of the deterministic model, suggesting the epidemic's extinction. A simulation was run using MATLAB (see Appendix A) to investigate the impact of various parameters. Figure 5, generated from the first experiment, presents empirical data to support the model assumptions and conclusions.

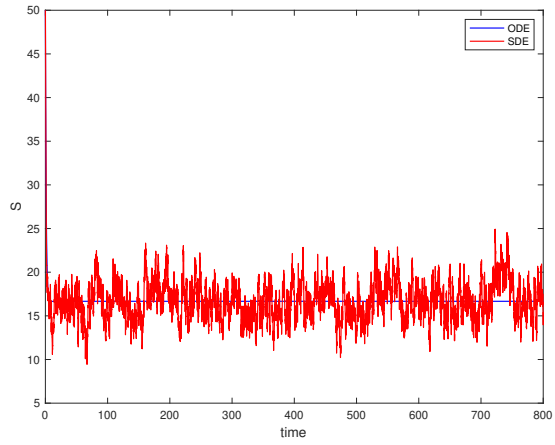

(a) Susceptible class

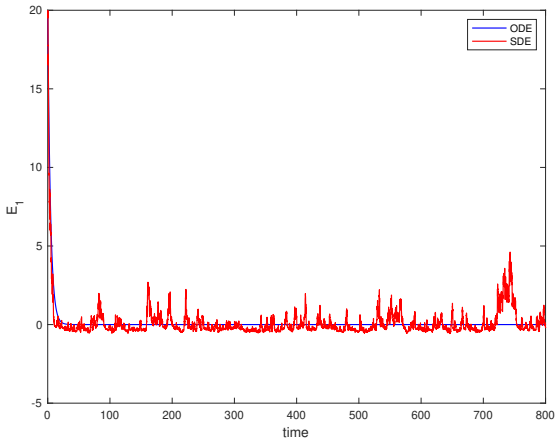

(b) Expose category 1

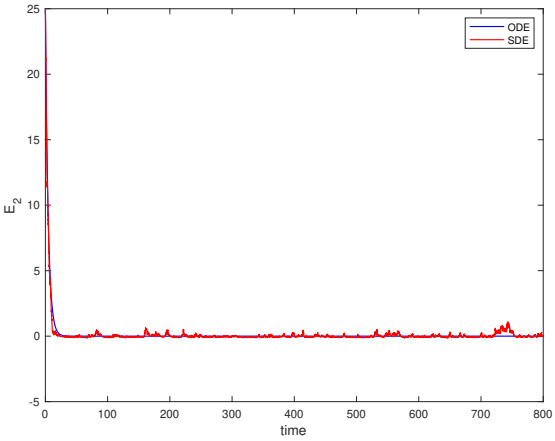

(c) Expose category 2

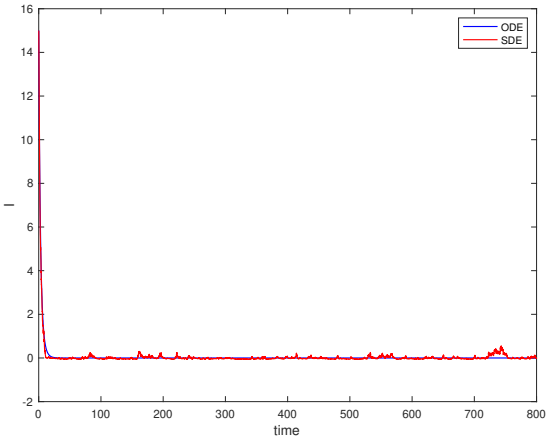

(d) Infectious class

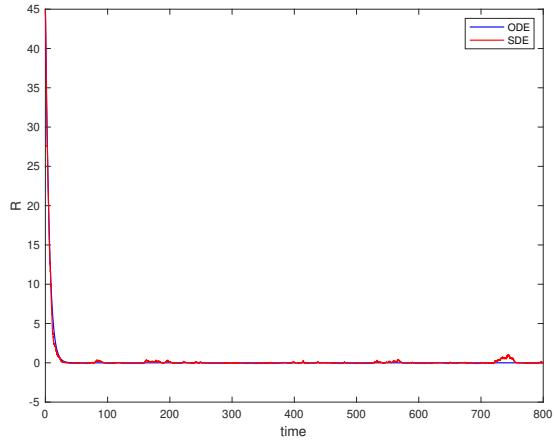

(e) Recovered class

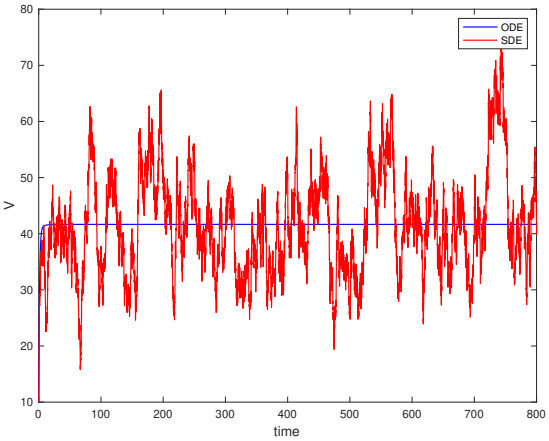

(f) Vaccinated class

Figure 5. The extinction of the system (2.2) and the system (2.3).

Table 2. The values of the parameters for model (2.3).

Parameters	Case 1	Case 2	Case 3
Π	10.0	10.5	10.5
β	0.05	0.80	0.80
η	0.05	0.01	0.01
p	0.45	0.30	0.30
q	0.05	0.30	0.30
λ_1	0.40	0.20	0.20
λ_2	0.20	0.30	0.30
γ	0.45	0.10	0.10
ω	0.45	0.20	0.20
σ	0.45	0.45	0.45
ξ_1	0.55	0.25	0.75
ξ_2	0.65	0.25	0.65
ξ_3	0.31	0.25	0.25
ξ_4	0.21	0.25	0.25
ξ_5	0.19	0.90	0.95
ξ_6	0.59	1.20	1.25
$\mathbf{S}(t)$	50.0	500	500
$\mathbf{E}_1(t)$	20.0	200	200
$\mathbf{E}_2(t)$	25.0	250	250
$\mathbf{I}(t)$	15.0	150	150
$\mathbf{R}(t)$	45.0	450	450
$\mathbf{V}(t)$	15.0	100	100

6.2. Numerical simulations for persistence

The dynamical analysis of a virus model in WSNs also exhibits the property of persistence. Here, by simulating the model, we noticed that a percentage of the nodes are always infected with the virus whenever the threshold value is larger than one. To be more precise, the simulation explains that infected and exposed nodes remain non-negative and are finally approaching a non-trivial steady state under the condition of $\mathbf{R}_0^P \approx 1.815$ if $\alpha_1 = 0.10$, $\alpha_2 = 0.10$, $\alpha_3 = 0.10$, $\alpha_4 = 0.15$, $\alpha_5 = 0.12$, and $\alpha_6 = 0.10$, so the malware will continue to exist within the networks. Figures 6(a)–6(f) show how the simulation analysis of the activity of malware in a network takes into consideration both geographical and temporal aspects. The computation of the stochastic model, which has a reproduction value of more than one, and the threshold associated with the deterministic system, which is also greater than one, is very simple (see Figure 6). Table 2 (Case 2) displays the system's parameters and initial settings (2.3). Changing the noise intensity value shows that the infection model (2.3) can persist, as seen in Figures 7(a)–7(f), where the $\mathbf{R}_0^P \approx 2.15$ if $\alpha_1 = 0.05$, $\alpha_2 = 0.05$, $\alpha_3 = 0.05$, $\alpha_4 = 0.05$, $\alpha_5 = 0.05$, and $\alpha_6 = 0.05$. The computation of the stochastically generated model, which has a threshold value of more than one, and the threshold associated with the deterministic system, which is also bigger than one, is rather simple. Table 2 (Case 3) shows the parameters and starting values for the system (2.3) in Figure 7.

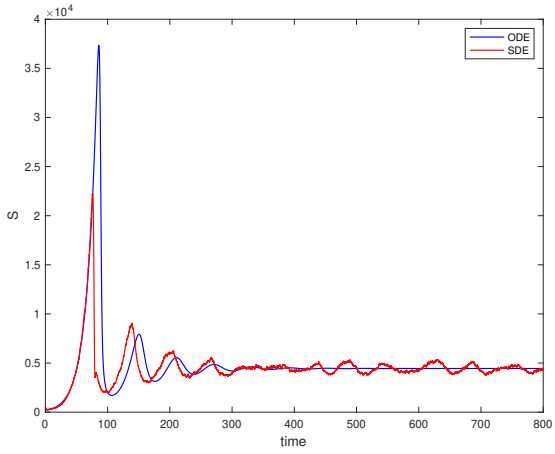

(a) Susceptible class

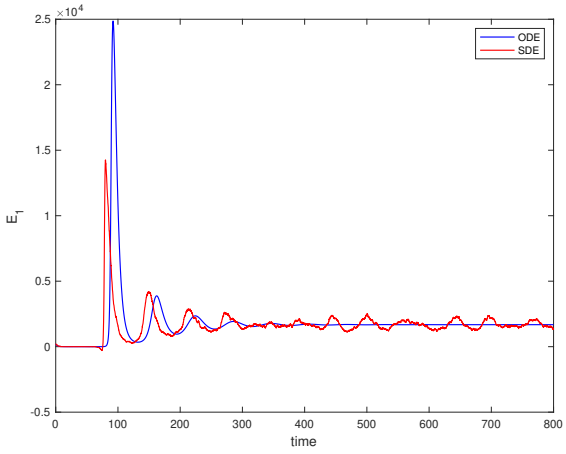

(b) Expose category 1

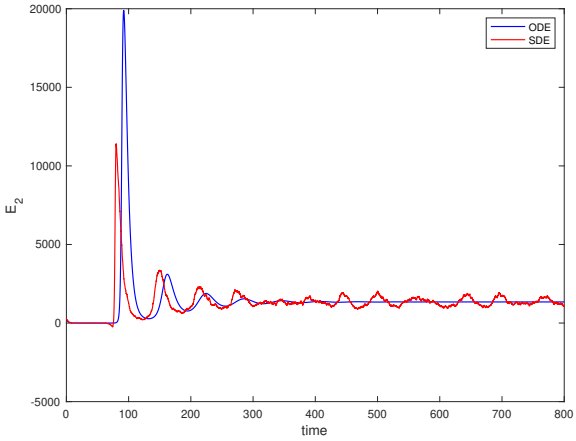

(c) Expose category 2

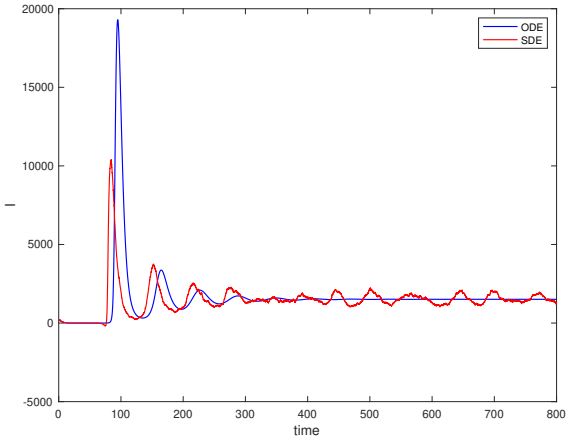

(d) Infectious class

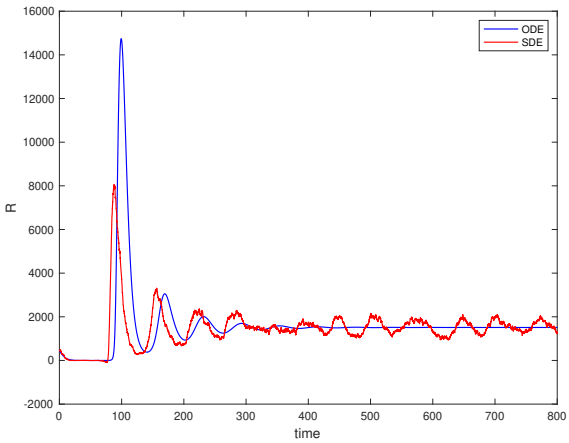

(e) Recovered class

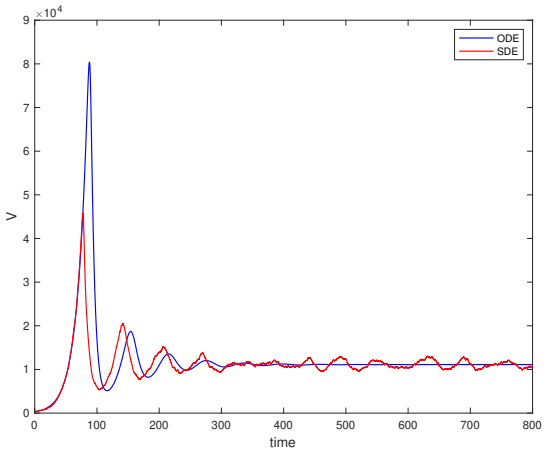

(f) Vaccinated class

Figure 6. Numerical simulations comparing the deterministic system (2.2) with the stochastic system (2.3).

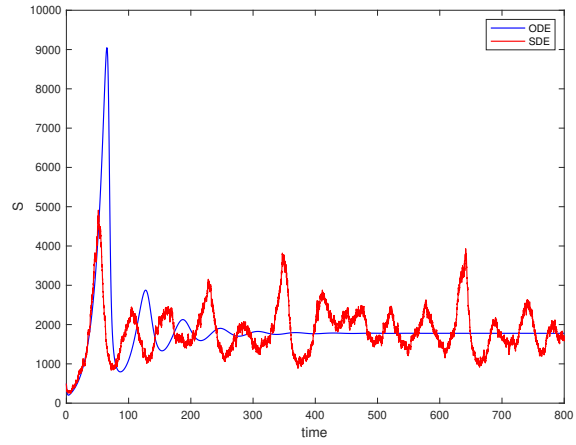

(a) Susceptible class

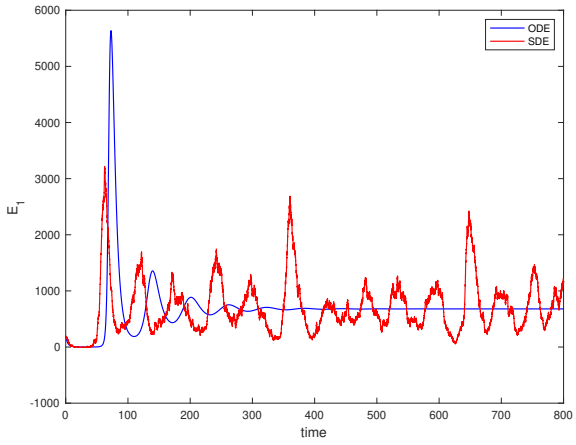

(b) Expose category 1

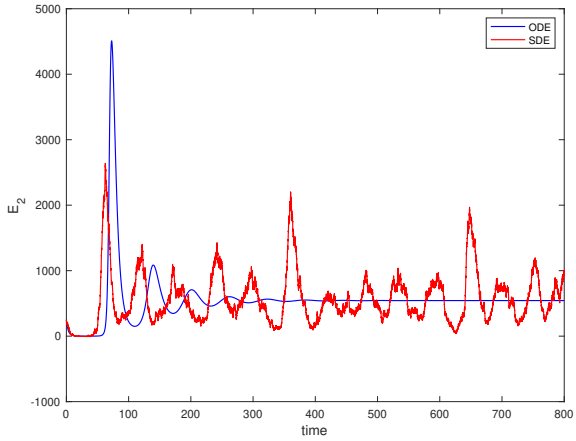

(c) Expose category 2

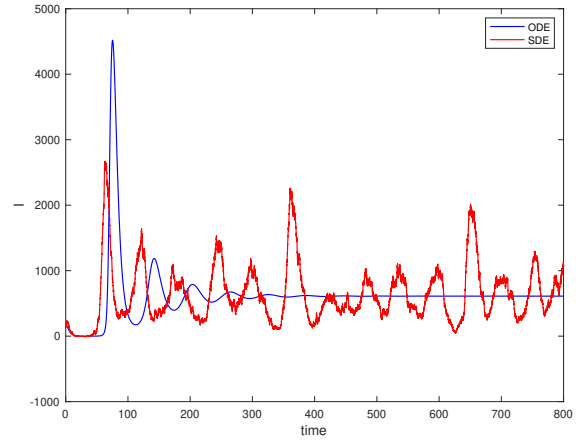

(d) Infectious class

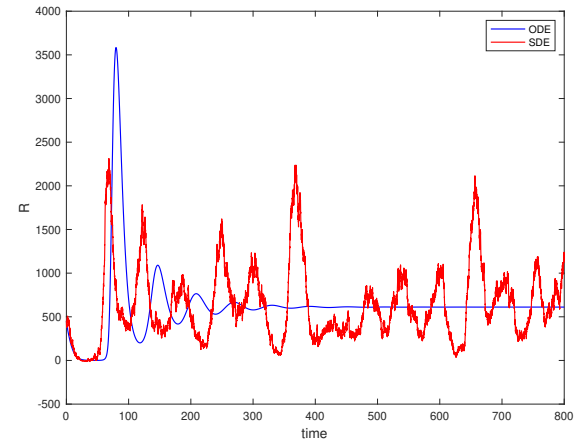

(e) Recovered class

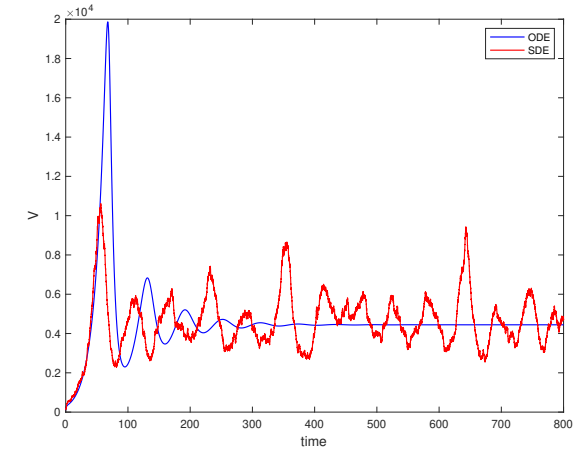

(f) Vaccinated class

Figure 7. The corresponding simulations of the deterministic system (2.2) and the system (2.3) when we change the parameters value and noise intensity.

6.3. Designed LMBNNs procedure

Let $Z(t) = [\mathbf{S}, \mathbf{E}_1, \mathbf{E}_2, \mathbf{I}, \mathbf{R}, \mathbf{V}]^\top \in \mathbb{R}^6$ be the state of system (2.3),

$$dZ(t) = f(Z(t))\,dt + \mathrm{diag}(\xi_1\mathbf{S}, \xi_2\mathbf{E}_1, \xi_3\mathbf{E}_2, \xi_4 I, \xi_5\mathbf{R}, \xi_6 V)\,d\mathbf{Q}(t) + \int_{\mathcal{X}} a(y, Z(t^-))\,\tilde{P}(d\chi),$$

where $f(\cdot)$ is the drift in system (2.3), $\mathbf{Q}(t)$ are independent Brownian motions, and $\tilde{P}$ the α compensated jump measure. We approximate the (mean) trajectory or solution operator by a feed-forward neural map

$$\widehat{Z}_\theta(t) = W_2\,\sigma(W_1\,\psi(t) + b_1) + b_2, \qquad \psi(t) = [t,\, Z(0)]^\top,$$

with parameters $\theta = \{W_1, W_2, b_1, b_2\}$ and activation $\sigma(\cdot)$ (log-sigmoid in our experiments). From M Monte–Carlo trajectories $\{Z^{(m)}(t_k)\}_{k=0}^K$ generated by the extended Milstein scheme (Section 6) under the chosen α-stable parameters, we formed the supervised set $\mathcal{D} = \{(t_k, Z^{(m)}(t_k))\}$. The Levenberg–Marquardt backpropagation neural networks (LMBNNs) approach is employed to analyze the dynamic behavior of the stochastic model delineated in system (2.3), and to physiologically characterize the transmission of the stochastic variant of HBV infection. The scheme is developed and implemented for three components of the model, with the results presented in the Figures 8–13. This picture illustrates the workflow diagram of the SKNov system, showcasing the design via two separate metrics: LMBNN-based procedures and mathematical processes. The dataset design utilizes the Adam method, allocating 82% for training and 9% for validation, as shown in Table 2 (Case 3). We utilized the log-sigmoid transfer function to examine the hidden layers and constructed a singular input-output layer configuration (comprising neurons). The ongoing neural network analysis is conducted meticulously to address challenges such as premature convergence, overfitting, and latent situations. Consequently, the network parameters were meticulously established based on experience, rigorous testing, and understanding. The parameter settings were meticulously adjusted, as even slight modifications could substantially impact the overall circumstances and the efficacy of the inquiry. In the MATLAB application, we utilized the NFTOOL command to execute the stochastic process employing LMBNNs, ensuring suitable configurations for hidden neuron sections, testing statistics, learning methodologies, and validation statistics. Table 2 (Case 3) presents the parameters employed to resolve the SKNov model using LMBNNs. The performance of the SKNov model is assessed by mean square error (MSE) and state evolution (SE), as seen in Figures 8–13. Figure 9 illustrates the regression results for Case 3 from Table 2, with a computed value of 1 signifying an ideal model.

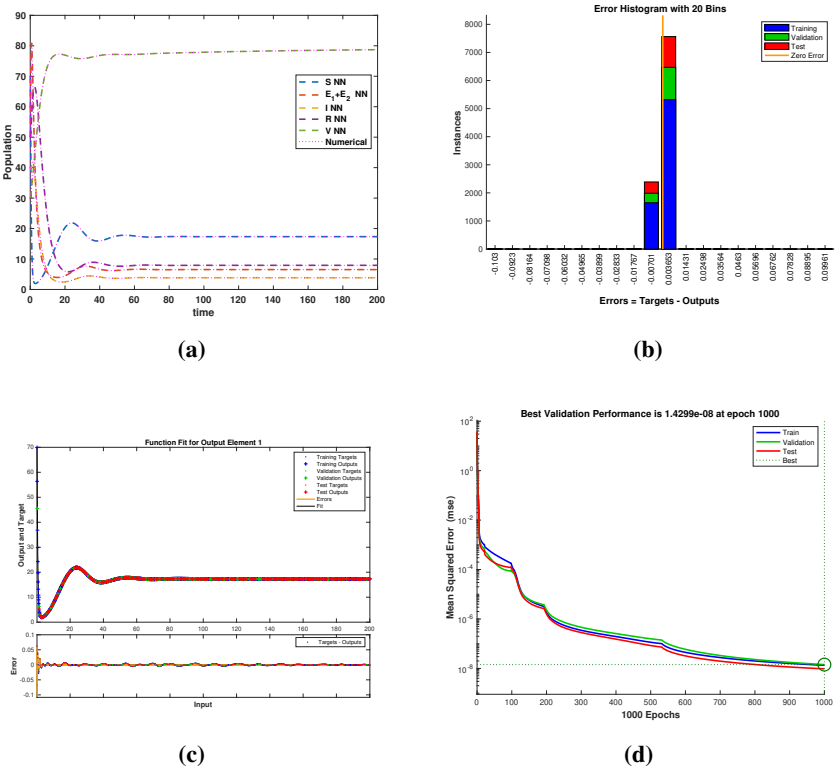

Figure 8. MSE and STs for the SKNov system (2.3).

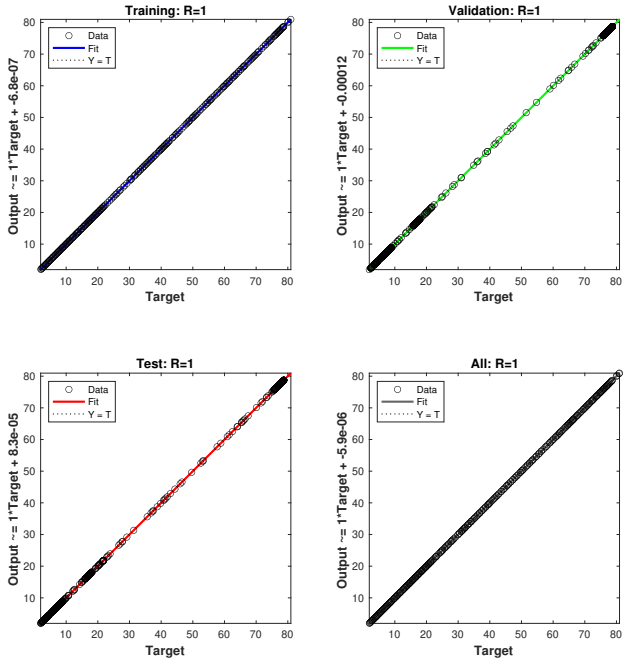

Figure 9. Regression for the SKNov system (2.3).

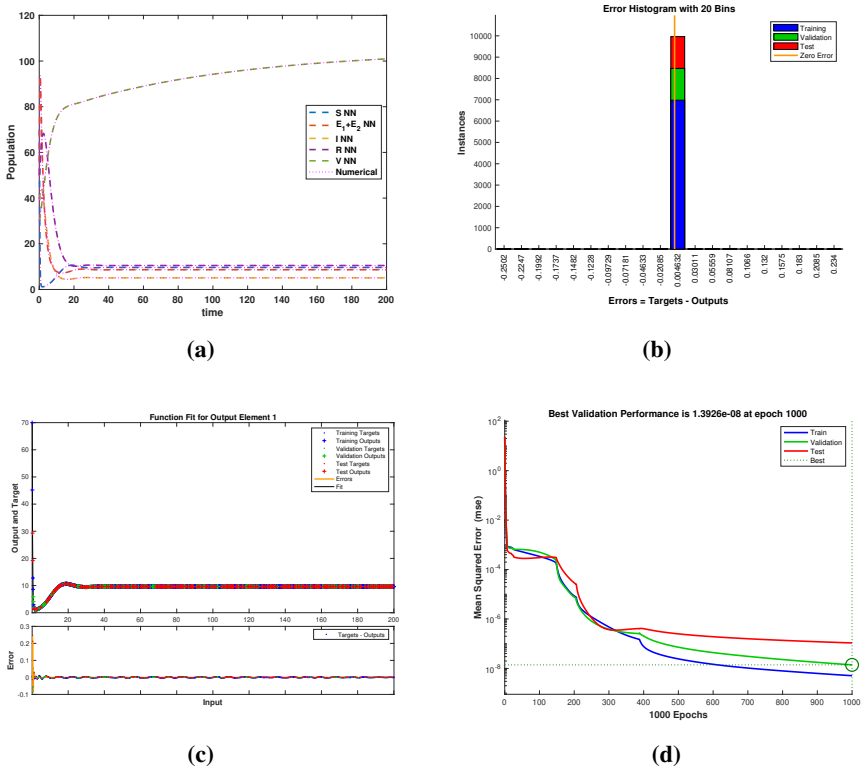

(a) **(b)**

(c) **(d)**

Figure 10. MSE and STs for the SKNov system (2.3).

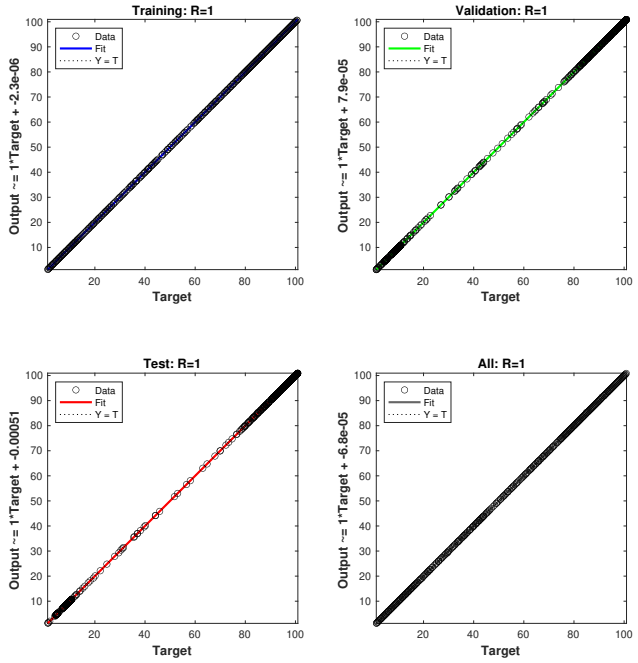

Figure 11. Regression for the SKNov system (2.3).

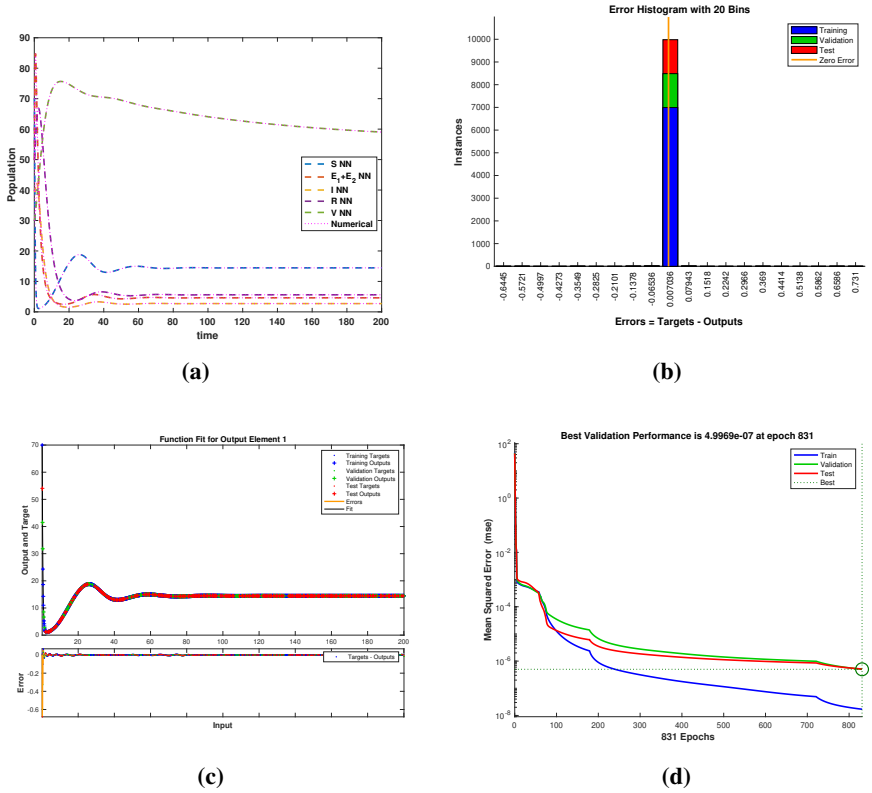

Figure 12. MSE and STs for the SKNov system (2.3).

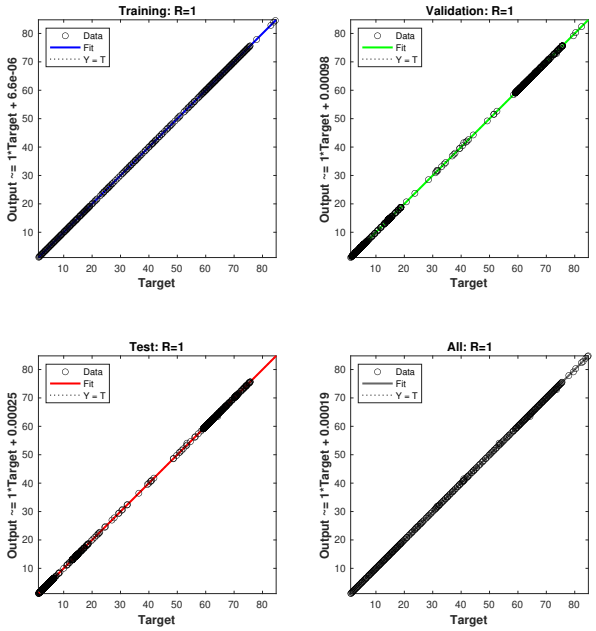

Figure 13. Regression for the SKNov system (2.3).

7. Conclusions

In this work, we formulated and analyzed a stochastic $\mathbf{SE_1E_2IRV}$ model to explore the dynamics of the computer virus within WSNs accounting for the unpredictability of nodes and anti-virus applications. The key purpose of the study was to explain the effect of environmental fluctuations on WSNs and to reduce the malware spread within the networks. The model was formulated on the basis of certain assumptions while including Gaussian white noise and Leavy jumps. This method facilitates a more accurate depiction of the system's dynamics in unknown settings. We performed the stochastic stability, derived a six-dimensional Fokker-Planck equation, and obtained analytical representations of the probability density functions. Subsequently, we developed a scheme that implement these analytical representations pdf in MATLAB. The behavior of the model around the quasi-endemic state was numerically investigated, and the results reflect the distinctive novelty of this research. Various parameter settings were used to generate graphical results to show the authenticity of the analytical results and to explain the complex aspects of the underlying problem. The results suggest that a numerical analysis of the model given by system (2.3) is necessary, and further studies can be conducted on control strategies, the rate of convergence, and other related topics. The significant outcomes of this study provide robust evidence that the proposed paradigm might enhance network longevity and data efficiency. These findings hold practical significance for software organizations, enabling them to leverage this information to create more efficient antivirus software that can successfully mitigate malware attacks in WSNs. Furthermore, the study will aid end-users in restoring corrupted nodes and deploying antivirus software on sensor nodes with meticulous attention, consequently enhancing the entire security framework to reduce assaults.

Future research areas may include the analysis of additional factors, such as isolated and quarantined nodes, as well as the integration of heterogeneous and mobile nodes. These characteristics enhance the model's applicability and provide greater insights into the dynamics of worm spread and mitigation strategies in WSNs.

Author contributions

Hassan Tahir: methodology, software, formal analysis, writing-original draft; Anwarud Din: Investigation, writing-original draft; Wajahat Ali Khan: resources, visualization, writing-review & editing; Mati ur Rahman: funding acquisition, supervision, writing-review & editing. All authors have read and approved the final version of the manuscript for publication.

Use of Generative-AI tools declaration

The authors declare they have not used Artificial Intelligence (AI) tools in the creation of this article.

Acknowledgments

This work was supported and funded by the Deanship of Scientific Research at Imam Mohammad Ibn Saud Islamic University (IMSIU) (grant number IMSIU-DDRSP2504).

Funding

This work was supported and funded by the Deanship of Scientific Research at Imam Mohammad Ibn Saud Islamic University (IMSIU) (grant number IMSIU-DDRSP2504).

Conflict of interest

The authors have no conflicts of interest.

References

1. Y. Y. Ghadi, T. Mazhar, T. Al Shloul, T. Shahzad, U. A. Salaria, A. Ahmed, et al., Machine learning solutions for the security of wireless sensor networks: A review, *IEEE Access*, **12** (2024), 12699–12719. https://doi.org/10.1109/access.2024.3355312
2. D. M. G. Preethichandra, L. Piyathilaka, U. Izhar, R. Samarasinghe, L. C. De Silva, Wireless body area networks and their applications: A review, *IEEE Access*, **11** (2023), 9202–9220. https://doi.org/10.1109/ACCESS.2023.3239008
3. M. Faris, M. N. Mahmud, M. F. M. Salleh, A. Alnoor, Wireless sensor network security: A recent review based on state-of-the-art works, *Int. J. Eng. Bus. Manag.*, **15** (2023), 1–29. https://doi.org/10.1177/18479790231157220
4. H. K. Patil, T. M. Chen, Wireless sensor network security, In: *Computer and information security handbook*, 2 Eds., San Francisco: Morgan Kaufmann, 2013, 301–322. https://doi.org/10.1016/B978-0-12-394397-2.00016-7
5. N. U. Nilabar, A. Manikandan, C. Venkataramanan, R. Dhanapal, A score based link delay aware routing protocol to improve energy optimization in wireless sensor network, *J. Eng. Res.*, **11** (2023), 404–413. https://doi.org/10.1016/j.jer.2023.100115
6. M. S. Haghighi, S. Wen, Y. Xiang, B. Quinn, W. L. Zhou, On the race of worms and patches: modeling the spread of information in wireless sensor networks, *IEEE T. Inf. Foren. Sec.*, **11** (2016), 2854–2865. https://doi.org/10.1109/tifs.2016.2594130
7. K. Das, V. Madhusudanan, M. H. Kabir, M. O. Gani, Stability analysis of E-epidemic SIT model with Beddington–DeAngelis functional response for wireless sensor network, *Discontinuity, Nonlinearity, and Complexity*, **12** (2023), 737–756. https://doi.org/10.5890/DNC.2023.12.003
8. T. Lenard, A. Collen, M. Benyahya, N. A. Nijdam, B. Genge, Exploring trust modelling and management techniques in the context of distributed wireless networks: A literature review, *IEEE Access*, **11** (2023), 106803–106832. https://doi.org/10.1109/access.2023.3320945
9. P. De, Y. H. Liu, S. K. Das, Deployment-aware modeling of node compromise spread in wireless sensor networks using epidemic theory, *ACM T. Sensor Network.*, **5** (2009), 1–33. https://doi.org/10.1145/1525856.1525861
10. Á. M. del Rey, A novel model for malware propagation on wireless sensor networks, *Math. Biosci. Eng.*, **21** (2024), 3967–3998. https://doi.org/10.3934/mbe.2024176

11. H. Tahir, A. Din, K. Shah, B. Abdalla, T. Abdeljawad, Advances in stochastic epidemic modeling: tackling worm transmission in wireless sensor networks, *Math. Comp. Model. Dyn.*, **30** (2024), 658–682. https://doi.org/10.1080/13873954.2024.2396480
12. S. M. A. Shah, H. Tahir, A. Khan, W. A. khan, A. Arshad, Stochastic model on the transmission of worms in wireless sensor network, *Journal of Mathematical Techniques in Modeling*, **1** (2024), 75–88. https://doi.org/10.56868/jmtm.v1i1.31
13. Y. S. Liu, X. W. Dong, E. Zio, Y. Cui, Active resilient secure control for heterogeneous swarm systems under malicious cyber-attacks, *IEEE Transactions on Systems Man and Cybernetics Systems*, **2025** (2025), 1–10. https://doi.org/10.1109/tsmc.2025.3580940
14. G. Xu, X. Y. Fan, S. Y. Xu, Y. B. Cao, X.-B. Chen, T. Shang, et al., Anonymity-enhanced sequential multi-signer ring signature for secure medical data sharing in IoMT, *IEEE T. Inf. Foren. Sec.*, **20** (2025), 5647–5662. https://doi.org/10.1109/tifs.2025.3574959
15. V. Gowdhaman, R. Dhanapal, Hybrid deep learning-based intrusion detection system for wireless sensor network, *International Journal of Vehicle Information and Communication Systems*, **9** (2024), 239–255. https://doi.org/10.1504/ijvics.2024.139627
16. S. Y. Chen, H. B. Jiang, J. Y. Hu, T. Y. Zheng, M. Y. Wang, Z. Xiao, et al., Echoes of fingertip: unveiling POS terminal passwords through Wi-Fi beamforming feedback, *IEEE T. Mobile Comput.*, **24** (2024), 662–676. https://doi.org/10.1109/tmc.2024.3465564
17. C. Rattanakul, I. Chaiya, A mathematical model for predicting and controlling COVID-19 transmission with impulsive vaccination, *AIMS Mathematics*, **9** (2024), 6281–6304. https://doi.org/10.3934/math.2024306
18. J. J. Du, C. L. Qin, Y. X. Hui, Optimal control and analysis of a stochastic SEIR epidemic model with nonlinear incidence and treatment, *AIMS Mathematics*, **9** (2024), 33532–33550. https://doi.org/10.3934/math.20241600
19. B. Li, H. J. Liang, Q. Z. He, Multiple and generic bifurcation analysis of a discrete Hindmarsh–Rose model, *Chaos Soliton. Fract.*, **146** (2021), 110856. https://doi.org/10.1016/j.chaos.2021.110856
20. A. Haghighi, N. Nyamoradi, Dynamics of a stochastic epidemic model for infectious diseases: inclusion of the environmental contamination factor, *J. Appl. Math. Comput.*, (2025). https://doi.org/10.1007/s12190-025-02507-y
21. P. J. Liu, A. Din, Comprehensive analysis of a stochastic wireless sensor network motivated by Black–Karasinski process, *Sci. Rep.*, **14** (2024), 8799. https://doi.org/10.1038/s41598-024-59203-3
22. Q. T. Ain, Nonlinear stochastic cholera epidemic model under the influence of noise, *Journal of Mathematical Techniques in Modeling*, **1** (2024), 52–74.
23. Q. Liu, A. A. Aeshah, A. Din, Lévy impact on the transmission of worms in wireless sensor network: stochastic analysis, *Results Phys.*, **52** (2023), 106757. https://doi.org/10.1016/j.rinp.2023.106757

24. Z. W. Yin, Y. S. Tan, Threshold dynamics of stochastic SIRSW infectious disease model with multiparameter perturbation, *AIMS Mathematics*, **9** (2024), 33467–33492. https://doi.org/10.3934/math.20241597

25. Y. Q. Qiao, J. H. Lü, T. Wang, K. X. Liu, B. C. Zhang, H. Snoussi, A multihead attention self-supervised representation model for industrial sensors anomaly detection, *IEEE T. Ind. Inform.*, **20** (2024), 2190–2199. https://doi.org/10.1109/tii.2023.3280337

26. Z. G. Xiong, Q. Q. Lou, Y. F. Li, H. Chen, X. M. Zhang, Y. Li, et al., NDLSC: A new deep learning-based approach to smart contract vulnerability detection, *J. Sign. Process. Syst.*, **97** (2025), 49–68. https://doi.org/10.1007/s11265-025-01954-x

27. X.-B. Zhang, X.-D. Wang, H.-F. Huo, Extinction and stationary distribution of a stochastic SIRS epidemic model with standard incidence rate and partial immunity, *Physica A*, **531** (2019), 121548. https://doi.org/10.1016/j.physa.2019.121548

28. M. El Fatini, I. Sekkak, Lévy noise impact on a stochastic delayed epidemic model with Crowly–Martin incidence and crowding effect, *Physica A*, **541** (2020), 123315. https://doi.org/10.1016/j.physa.2019.123315

29. Y.-A. Dong, Y.-F. Dong, T.-T. Lin, Dynamics of a stochastic rumor propagation model incorporating media coverage and driven by Lévy noise, *Chinese Phys. B*, **30** (2021), 080201. https://doi.org/10.1088/1674-1056/ac0423

A. MATLAB Program

The following MATLAB code is the numerical scheme for solving the proposed system of stochastic differential equations.

```
N = 1000;
initS = 500;
initE1 = 200;
initE2 = 250;
initI = 150;
initR = 450;
initV = 100;
dt = 0.01;
time = 1000;
sim = 1;


lambda_jump = 0.1;
jump_magnitude = 0.05;

for k = 1:sim
    j = 1;
    S(j) = initS;
    E1(j) = initE1;
```

```
E2(j) = initE2;
I(j) = initI;
R(j) = initR;
V(j) = initV;
t(j) = dt;

while S(j) > 0 && t(j) < 1000

    kappa1 = phi - varphi * S(j) * I(j) / N - omega * S(j) -
       eta * S(j) + sigma * V(j);
    kappa2 = p * varphi * S(j) * I(j) / N - (lambda1 + eta) *
       E1(j);
    kappa3 = q * varphi * S(j) * I(j) / N - (lambda2 + eta) *
       E2(j);
    kappa4 = lambda1 * E1(j) + lambda2 * E2(j) - (gamma + eta)
       * I(j);
    kappa5 = gamma * I(j) - eta * R(j);
    kappa6 = omega * S(j) - eta * V(j);


    sigma1 = S(j);
    sigma2 = E1(j);
    sigma3 = E2(j);
    sigma4 = I(j);
    sigma5 = R(j);
    sigma6 = V(j);


    rn = randn;


    jump_indicator = poissrnd(lambda_jump * dt);
    jump_value = jump_indicator * jump_magnitude * (2 * rand -
       1);


    S(j + 1) = S(j) + kappa1 * dt + eta1 * sqrt(sigma1) * sqrt(
       dt) * rn + jump_value;
    E1(j + 1) = E1(j) + kappa2 * dt + eta2 * sqrt(sigma2) *
       sqrt(dt) * rn + jump_value;
    E2(j + 1) = E2(j) + kappa3 * dt + eta3 * sqrt(sigma3) *
       sqrt(dt) * rn + jump_value;
```

```
        I(j + 1) = I(j) + kappa4 * dt + eta4 * sqrt(sigma4) * sqrt(
           dt) * rn + jump_value;
        R(j + 1) = R(j) + kappa5 * dt + eta5 * sqrt(sigma5) * sqrt(
           dt) * rn + jump_value;
        V(j + 1) = V(j) + kappa6 * dt + eta6 * sqrt(sigma6) * sqrt(
           dt) * rn + jump_value;


        t(j + 1) = t(j) + dt;
        j = j + 1;
    end
end


S1(1) = initS;
E11(1) = initE1;
E21(1) = initE2;
I1(1) = initI;
R1(1) = initR;
V1(1) = initV;

for k = 1:time / dt
    S1(k + 1) = S1(k) + dt * (phi - varphi * S1(k) * I1(k) / N -
       omega * S1(k) - eta * S1(k) + sigma * V1(k));
    E11(k + 1) = E11(k) + dt * (p * varphi * S1(k) * I1(k) / N - (
       lambda1 + eta) * E11(k));
    E21(k + 1) = E21(k) + dt * (q * varphi * S1(k) * I1(k) / N - (
       lambda2 + eta) * E21(k));
    I1(k + 1) = I1(k) + dt * (lambda1 * E11(k) + lambda2 * E21(k) -
        (gamma + eta) * I1(k));
    R1(k + 1) = R1(k) + dt * (gamma * I1(k) - eta * R1(k));
    V1(k + 1) = V1(k) + dt * (omega * S1(k) - eta * V1(k));
end
```

AIMS Press